

Trial Wavefunctions for $\nu = \frac{1}{2} + \frac{1}{2}$ Quantum Hall Bilayers

Gunnar Möller,¹ Steven H. Simon² and Edward H. Rezayi³

¹ TCM Group, Cavendish Laboratory, J. J. Thomson Ave., Cambridge CB3 0HE, UK

² Bell Laboratories, Alcatel-Lucent, Murray Hill, New Jersey 07974

³ Department of Physics, California State University, Los Angeles, California 90032

(Dated: November 25th, 2008)

Quantum Hall bilayer systems at filling fractions near $\nu = \frac{1}{2} + \frac{1}{2}$ undergo a transition from a compressible phase with strong intralayer correlation to an incompressible phase with strong interlayer correlations as the layer separation d is reduced below some critical value. Deep in the intralayer phase (large separation) the system can be interpreted as a fluid of composite fermions (CFs), whereas deep in the interlayer phase (small separation) the system can be interpreted as a fluid of composite bosons (CBs). The focus of this paper is to understand the states that occur for intermediate layer separation by using trial variational wavefunctions. We consider two main classes of wavefunctions. In the first class, previously introduced in Möller *et al.* [Phys. Rev. Lett. **101**, 176803 (2008)], we consider interlayer BCS pairing of two independent CF liquids. We find that these wavefunctions are exceedingly good for $d \approx \gamma_0$ with γ_0 the magnetic length. The second class of wavefunctions naturally follows the reasoning of Simon *et al.* [Phys. Rev. Lett. **91**, 046803 (2003)] and generalizes the idea of pairing wavefunctions by allowing the CFs also to be replaced continuously by CBs. This generalization allows us to construct exceedingly good wavefunctions for interlayer spacings of $d \approx \gamma_0$, as well. The accuracy of the wavefunctions discussed in this work, compared with exact diagonalization, approaches that of the celebrated Laughlin wavefunction.

I. INTRODUCTION

In bilayer quantum Hall systems at filling fraction $\nu = \frac{1}{2} + \frac{1}{2}$, at least two different quantum states of matter are known to occur, depending upon the spacing d between the layers.¹ For large enough spacing, the two layers interact very weakly and must be essentially independent $\nu = \frac{1}{2}$ states, which can be described as compressible composite fermion (CF) Fermi seas.² So long as the distance between the two layers is very large, there are very strong intralayer correlations but very weak interlayer correlations (although, as we will discuss below, even very weak interlayer correlations may create a pairing instability at exponentially low temperatures³). Conversely, for small enough spacing between the two layers the ground state is known to be the interlayer coherent “111 state”, which we can think of as a composite boson (CB), or interlayer exciton condensate,⁴ with strong interlayer correlations and intralayer correlations which are weaker than those of the composite fermion Fermi sea.¹ While the nature of these two limiting states is reasonably well understood, the nature of the states at intermediate d is less understood and has been an active topic of both theoretical^{3,5,6,7,8,9,10,11,12,13,14,15,16} and experimental interest.^{17,18,19,20,21,22,23,24,25,26,27} Although there are many interesting questions remaining that involve more complicated experimental situations, within the current work we always consider a zero temperature bilayer system with zero tunnelling between the two layers and no disorder. Furthermore, we only consider the situation of $\nu = \frac{1}{2} + \frac{1}{2}$ where the electron density in each layer is such that $n_1 = n_2 = B = 2\phi_0$ with $\phi_0 = hc/e$ the flux quantum and B the magnetic field. Finally we assume that electrons are fully spin-polarized, we neglect the finite extension of the wave functions in the z -direction, and we always assume that the magnetic field is precisely perpendicular to the plane of the sample.

Our main focus in this work is on the nature of the transition between interlayer 111 (CB) state and the intralayer

Fermi liquid (CF) state. Currently, contradictory conclusions about the nature of the transition may be drawn from the literature. The experiments are complex and are frequently hard to interpret (and may require assumptions beyond the simplifying assumptions made in the current paper). While some of the experiments^{17,18,19,20,21,22} point towards a continuous transition between two phases, it is not clear whether this could actually be a first order transition smeared by disorder.⁸ There is no doubt, however, that a notable change of behavior takes place in the approximate vicinity of $d = \gamma_0 \approx 1.7$ with $\gamma_0 = \frac{p}{\phi_0} = \frac{B}{B}$ as the magnetic length.

Theoretically, the situation has also remained unclear. Several theoretical works^{6,28,29} found indications of a first order transition near $d = \gamma_0 \approx 1.3$, whereas others have found no indication for a first order transition and evoke a continuous evolution of correlations,¹⁰ and indications of a continuous transition occurring near $d = \gamma_0 \approx 1.6$.³⁰

Description of the phases that occur in the bilayer system has also been quite a challenge. Some very influential works have pointed to the possibility that a number of exotic phases could be lurking within this transition as well.^{3,9,10,11,14,31} In particular, it has been suggested^{3,11,12} that the bilayer CF Fermi sea is always unstable to BCS pairing from weak interactions between the two layers (due to gauge field fluctuations). Some of these works^{11,12} further concluded that the pairing of CFs should be in the $p_x - ip_y$ channel, which would be analogous to the pairing that occurs in single layer CF systems to form the Moore-Read Pfaffian state^{32,33} from the CF Fermi sea. However, these works did not provide any numerical evidence supporting these claims.

Recent work by the current authors¹³ has shed considerable light on the subject. In this work, compelling numerical evidence was given that for $d = \gamma_0 \approx 1$ the ground state is well described as a CF-BCS paired phase, although the pairing channel is $p_x + ip_y$ rather than the previously predicted $p_x - ip_y$. Explicit pairing wavefunctions were shown to have extremely

high overlaps with the exact ground state for small systems. This work will be described in more detail below.

A somewhat different approach has also been proposed by some of the present authors and collaborators³⁴ in order to understand the transition between the phase at large d and the 111, or CB phase at small d . In that work, a set of trial wavefunctions was constructed to attempt to describe the crossover. This theory (to be discussed in depth below) provides an intuitive picture for the transition from the CF-liquid product state to the 111-state in terms of an energy trade-off between intralayer interaction energy and interlayer interaction energy. At large layer separation d , CFs fill a Fermi sea. These CFs can be thought of as electrons bound to a pair of correlation holes within the same layer. At small layer separation the 111-state can be thought of as a condensate of interlayer excitons or composite bosons. These composite bosons are formed by electrons bound to a correlation hole in the opposite layer, which is in fact a true hole of charge $+e$, just as a Laughlin quasihole on top of a $\nu = 1$ quantum Hall liquid. Additionally, CBs carry a single correlation hole in the same layer. Within the theory of Ref. 34, at intermediate d wavefunctions were introduced with some density of CFs having particle-hole binding within the layer and some density of CBs having particle-hole binding between layers. As the distance d between the layers is continually reduced, the CFs are continually replaced by CBs and the intralayer correlation is replaced by interlayer correlations.

While physically appealing, this description of the transition is clearly incomplete in that it considers CFs and CBs as independent types of particles, though in reality all of the electrons must be identical. Both the CFs and CBs consist of electrons bound to correlation holes or vortices, or with “flux attached” in the Chern-Simons language. The difference between the CBs and CFs is whether they are bound to correlation holes in the opposite layer (CBs) or only within the same layer (CFs). However, nothing prevents electrons from breaking free from their correlation holes and becoming bound to a different correlation hole — which could then change the identity of a particle from a CB to a CF and vice versa. Indeed, whenever two composite bosons in opposite layers approach the same coordinate position, they can “trade” their accompanying correlation holes (vortices or flux quanta), and emerge as two composite fermions. In terms of a second quantized notation, with ψ representing a composite fermion annihilation operator, and ϕ representing a composite boson annihilation operator, such scattering processes would be described by an interaction term

$$\lambda_{\mathbf{k}_1 \mathbf{k}_2 \mathbf{k}_3 \mathbf{k}_4} \psi_{\mathbf{k}_1}^\dagger \psi_{\mathbf{k}_2}^\dagger \phi_{\mathbf{k}_3} \phi_{\mathbf{k}_4} + h.c. \quad (1)$$

with \mathbf{n} and $\mathbf{\#}$ representing the two layers and λ as a coupling constant (and $h.c.$ denoting the hermitian conjugate). If the bosons happen to be condensed, there is a large expectation for the CBs to be in a $\mathbf{k} = 0$ state. Invoking momentum conservation, the most dominant such interaction term is then of the form

$$\lambda_{\mathbf{k}} \psi_{\mathbf{k}_1}^\dagger \psi_{\mathbf{k}_1}^\dagger \phi_{\mathbf{k}-\mathbf{0}} \phi_{\mathbf{k}-\mathbf{0}} + h.c. \quad (2)$$

which we immediately recognize as a pairing term for the composite fermions. Thus we see that the mixed CF-CB picture is quite closely linked to the idea of CFs forming a CF-BCS state.

As discussed above, our numerics indicate that CF pairing occurs in the $p_x + ip_y$ channel. An equivalent statement is that the two-CF pair wavefunction acquires a phase of $+2\pi$ as two paired electrons in opposite layers are taken in a clockwise path around each other. We will further argue that this is the only pairing symmetry that is compatible with coexistence of CFs and CBs. The argument rests on the fact that for the 111 wavefunction, taking any electron around any other electron in the opposite layer will result in a $+2\pi$ phase. As will be further illustrated below, compatibility of CBs that make up the 111 state with the CFs that compose the p -wave paired CF state requires that these phases match, and will require that the p -wave pairing is of $p_x + ip_y$ type.

In the current work, we construct explicit wavefunctions for interlayer paired CF states. As in BCS theory, the shape of the pairing wavefunction is treated in terms of a set of (a very small number of) variational parameters. As previously discussed in Ref. 13 we find that for interlayer spacings $d \gg \gamma_0$ our trial states are exceedingly good representations of the ground state. However, at spacings below $d \approx \gamma_0$ we find that the simple paired CF states are no longer accurate. We then return to the above described idea of CF-CB mixtures. With only one additional variational parameter representing the probability that an electron is a CB versus being a CF, we obtain a family of wavefunctions that nearly match the exact ground state for all values of $d = \gamma_0$.

The general structure of this paper is as follows. In section II, we will discuss in detail the particular wavefunctions to be studied. First, in section II A we review the composite fermion Fermi liquid in single layer systems, and focus on some particular aspects that help us construct bilayer states with paired CFs, previously introduced in Ref. 13, in section II B. We then turn to the discussion of the interlayer coherent 111-state in section II C and how it too can be interpreted as both a state of composite bosons (CBs) and as a paired state. In section II D we discuss the merging of the physics of CBs with that of the paired CF states to yield a mixed fluid wavefunction which incorporates both types of physics. Crucially, we show in this section that $p_x + ip_y$ is the only pairing symmetry of CFs that can coexist with CBs. We note that wavefunctions discussed in section II D include the mixed CB-CF wavefunctions of Ref. 34 as a special case.

Having constructed a family of variational wavefunctions, we proceed to test the validity of this approach based on numerical calculations on the sphere presented in section III. Data from Monte-Carlo simulations of the paired CF and mixed fluid wavefunctions is compared with data obtained from exact numerical diagonalizations of the Coulomb Hamiltonian for model systems of up to 14 electrons in sections III A and III B. In section III C, we discuss the properties of the various trial states via the occupation of CF orbitals and in analogy to a BCS superconductor. Section III D is devoted to a discussion of order parameters that characterize the system. In Section IV we further discuss our understanding and

interpretation of our results. We also briefly discuss a number of issues including the effects of finite temperature, layer density imbalance, tunneling between the layers, and electron spin. Consequences for electronic transport are also analyzed. Finally we discuss the expected transport properties of the phases we describe. In section V we conclude and briefly summarize our results.

We have relegated to the appendices a number of details that are not in the main development of the paper. In Appendix A, we discuss in detail how to adapt the mixed fluid wavefunctions to obtain a representation on the sphere. More numerical results for a restricted class of wave functions, corresponding to filled CF shells on the sphere, are discussed in Appendix B. Further details about the procedure applied for the optimization of trial states are elaborated in Appendix C. Finally, Appendix D discusses some properties of the two-electron correlation functions in the bilayer system.

II. WAVEFUNCTIONS FOR THE QUANTUM HALL BILAYER

In this section we review the various trial wavefunctions that we will be studying throughout this paper. To the experienced reader the discussion of the composite fermion liquid (section II A) and the 111 state (section II C) will be mostly review. This material is nonetheless included in depth to emphasize a few key points that guide our reasoning.

For simplicity, in this section we will consider infinite-sized systems on a planar geometry so that we can write wavefunctions in the usual complex coordinate notation. Here and in the following, $z_i = x_i + iy_i$ is the complex representation of the coordinates of particle i (with the overbar representing the complex conjugate), and the usual Gaussian factors of $e^{-\sum_i z_i \bar{z}_i / 2\ell_0^2}$ are understood to be included in the measure of the Hilbert space and will not be written explicitly for simplicity of notation. For bilayer states, we note coordinates in the second layer as w_j , using the same complex representation. In section III below, we will convert to considering wavefunctions on the sphere, where we actually perform our numerical calculations. The changes required to adapt our theory to the spherical geometry are discussed in Appendix A.

A. Composite Fermion Liquid

For bilayer systems at infinite layer spacing, the interlayer interaction vanishes and the two layers can be considered as independent $\nu = \frac{1}{2}$ systems. For such single layer $\nu = \frac{1}{2}$ systems, the composite fermion approach² has been remarkably successful in describing a great deal of the observed physics. In this picture,^{2,35} the wave function for interacting electrons in magnetic field B is written in terms of the wavefunction for free (composite) fermions in an effective magnetic field $\mathcal{B} = B - 2n\phi_0$ with the density of electrons n . Each fermion is also attached to two vortices (or correlation holes) of the wavefunction (Jastrow factors) resulting in the following type

of wavefunction:

$$\Psi^{CF} = \mathcal{P}_{\text{LLL}} \prod_{k < p} (z_p - \bar{z}_k)^2 \det [\phi_i(z_j; \bar{z}_j)]: \quad (3)$$

where ϕ_i are the orbitals for free fermions in the effective magnetic field \mathcal{B} , and \mathcal{P}_{LLL} is the projection operator that projects to the lowest Landau level. The determinant in equation (3) above describes a Slater determinant of electrons at z_i filling states given by the orbitals ϕ_i .

For the special case $\nu = \frac{1}{2}$ the CFs experience zero effective field and behave similarly as electrons at zero field, forming a Fermi sea.^{2,36,37} For an infinitely extended plane, plane waves form a basis of single particle orbitals for particles in zero effective magnetic field such that

$$\phi_i(z_j) = e^{ik_j \cdot r_j} \quad (4)$$

Since $\mathbf{k} = \frac{1}{2} (k\bar{z} + \bar{k}z)$ (with k being the complex representation of the vector \mathbf{k}) and the projection on the LLL transforms $\bar{z} \rightarrow 2\frac{\partial}{\partial z}$, the plane wave factors become translation operators under projection.³⁸ This yields

$$\Psi_{\frac{1}{2}} = \mathcal{A} \prod_{i < j} [z_i + \frac{1}{2}k_i] [z_j + \frac{1}{2}k_j]^2 \prod_i e^{ik_i z_i} \quad ; \quad (5)$$

where \mathcal{A} is the antisymmetrizing operator that sums over all possible pairings of the z_i 's with the k_j 's, odd permutations added with a minus sign. We see that the fermions are still bound to zeros of the wavefunction, but the positions of the zeros (correlation holes) are moved away from the electrons by a distance $\frac{1}{2}k$, which is given in terms of "momentum" k . In order to minimize the Coulomb energy, these distances should be minimized, but simultaneously, all the k_i have to be different or the wavefunction will vanish on antisymmetrization. Thus, to minimize potential energy, the k_i 's fill up a Fermi sea of minimal size. This is how the potential energy becomes the driving force for establishing the Fermi sea. Although this naive picture of charged dipole dynamics is not strictly true in the way that it is presented here,³⁹ there are several ways to more rigorously embody this type of dipolar Fermi sea dynamics in a theory of the lowest Landau level, which give credibility to this type of simplified argument.^{40,41,42}

Unfortunately, the projection \mathcal{P} in Eq. 3 is exceedingly difficult to implement numerically for large systems. To circumvent this problem, Jain and Kamilla⁴³ proposed a rewriting of the composite fermion wavefunction as

$$\Psi^{CF} = \prod_{k < p} (z_p - \bar{z}_k)^2 \det [\tilde{\phi}_i(z_j)] \quad ; \quad (6)$$

where

$$\tilde{\phi}_i(z_j) = J_j^{-1} \mathcal{P}_{\text{LLL}} [\phi_i(z_j; \bar{z}_j) J_j] \quad ; \quad (7)$$

with $J_j = \prod_{k \in j} (z_k - \bar{z}_j)$ and the ϕ_i chosen such as to represent wavefunctions corresponding to a filled Fermi sea.⁴⁴ This form, while not strictly identical to the form of Eq. 3, is extremely close numerically and has equally impressive overlaps

with exact diagonalizations⁴³ and is therefore an equally good starting point for studying composite fermion physics. However, in contrast to the form of Eq. 3, the form of Eqs. 6 and 7 are comparatively easy to evaluate numerically and therefore allow large system quantum Monte-Carlo calculations.⁴³ In this paper, we have used this type of approach.

In order to obtain a wavefunction for the bilayer system at $\nu = \frac{1}{2} + \frac{1}{2}$ and infinite layer separation, a simple product state of two composite fermion liquids (CFL) is appropriate.

$$\Psi(d \rightarrow \infty) = \Psi_{\text{CFL}}^{\text{upper}} \Psi_{\text{CFL}}^{\text{lower}} \quad (8)$$

At finite layer separation, however, correlations between the layers are expected to exist and have been suspected to resemble a paired state.^{3,11,12,31,45} As we will see below, the product state (8) may be regarded as a particular paired state whenever the Fermi-surface is inversion symmetric with respect to $\mathbf{k} = 0$, i.e., the center of the Fermi-sea. In these cases, for each particle in layer one occupying a state with momentum \mathbf{k} , there exists its partner in layer two occupying a state with momentum $-\mathbf{k}$.

B. Paired CF bilayer state

We now consider how to write a trial wavefunction for an interlayer paired composite fermion state, which we suggest should be an accurate description of the bilayer system when the spacing between the layers is large. The material in this section is mostly a review of material introduced in Ref. 13. As a starting point, let us take the well known BCS wavefunction in the grand canonical ensemble⁴⁶

$$\Psi_{\text{BCS}} = \prod_{\mathbf{k}} (u_{\mathbf{k}} + v_{\mathbf{k}} e^{i\varphi} a_{\mathbf{k}\#}^{\dagger} a_{-\mathbf{k}}^{\dagger}) \mathcal{D} \quad (9)$$

with the normalization $|u_{\mathbf{k}}|^2 + |v_{\mathbf{k}}|^2 = 1$ and where $a_{\mathbf{k}}^{\dagger}$ creates a particle in layer $\#$ with momentum \mathbf{k} . Note that the u 's and v 's are properly understood here as variational parameters of the BCS wavefunction. Next, we rewrite this wavefunction in an unnormalized form by multiplying all factors by $u_{\mathbf{k}}^{-1}$ and defining $g_{\mathbf{k}} = v_{\mathbf{k}}/u_{\mathbf{k}}$, so

$$\Psi_{\text{BCS}} = \prod_{\mathbf{k}} (1 + g_{\mathbf{k}} e^{i\varphi} a_{\mathbf{k}\#}^{\dagger} a_{-\mathbf{k}}^{\dagger}) \mathcal{D} \quad (10)$$

Finally, we project to a fixed number $2N$ of particles (i.e, switch to canonical ensemble) by integration over $d\varphi \exp(-iN\varphi)$ such that we retain exactly N pair creation operators. This yields

$$\Psi_{\text{BCS}} = \sum_{\{\mathbf{k}_1, \dots, \mathbf{k}_N\}} \prod_{\mathbf{k}_i} g_{\mathbf{k}_i} a_{\mathbf{k}_i\#}^{\dagger} a_{-\mathbf{k}_i}^{\dagger} \mathcal{D} \quad (11)$$

In the first quantized language, we can write

$$\Psi = \det [g(\mathbf{r}_{i\#}; \mathbf{r}_{j\#})] \quad (12a)$$

where g is the Fourier transform

$$g(\mathbf{r}_{i\#}; \mathbf{r}_{j\#}) = \sum_{\mathbf{k}} g_{\mathbf{k}} e^{i\mathbf{k} \cdot (\mathbf{r}_{i\#} - \mathbf{r}_{j\#})} \quad (12b)$$

Note that the exponential factor of the Fourier transform can be regarded as a product of two basis functions $\phi_{\mathbf{k}}(\mathbf{r}) = e^{i\mathbf{k}\cdot\mathbf{r}}$ on the plane, i.e.

$$e^{i\mathbf{k} \cdot (\mathbf{r}_{i\#} - \mathbf{r}_{j\#})} = e^{i\mathbf{k} \cdot \mathbf{r}_{i\#}} e^{-i\mathbf{k} \cdot \mathbf{r}_{j\#}} = \phi_{\mathbf{k}}(\mathbf{r}_{i\#}) \phi_{-\mathbf{k}}(\mathbf{r}_{j\#}) \quad (13)$$

With this in mind, similar paired wavefunctions can be written for more general geometries with arbitrary basis functions. In the following, we construct paired states for composite fermions in the bilayer system (denoting particles in the upper layer as z and those in the lower layer as w). As in section II A we will multiply our fermion wavefunction with composite-fermionizing Jastrow factors and project to the lowest Landau level yielding

$$\Psi = \mathcal{P}_{\text{LLL}} \left[\prod_{i < j} (z_i - z_j)^2 \prod_{i < j} (w_i - w_j)^2 \det [g(z_i; w_j)] \right] \mathcal{P}_{\text{LLL}} \det [J_i^{zz} J_j^{ww} g(z_i; w_j)] \quad (14)$$

where we have defined ‘‘single particle’’ Jastrow factors

$$J_i^{zz} = \prod_{k \in i} (z_i - z_k) \quad (15a)$$

$$J_i^{ww} = \prod_{k \in i} (w_i - w_k) \quad (15b)$$

In order to handle the projection numerically, we follow the recipe of Jain and Kamilla (7) discussed above, bringing the Jastrow factors inside the determinant and projecting individual matrix entries. This prescription applies to the bilayer case in a similar manner as for the single layer case (since the total Hilbert space of the bilayer system may be represented as a direct product of the space for each layer and projection in one space does not affect the other). We then obtain the final paired wave function:

$$\Psi^{\text{CF-BCS}} = \det [g_{\text{F}}(z_i; w_j)] \quad (16a)$$

where

$$g_{\text{F}}(z_i; w_j) = \sum_{\mathbf{k}} g_{\mathbf{k}} J_i^{zz} J_j^{ww} \tilde{\phi}_{\mathbf{k}}(z_i) \tilde{\phi}_{-\mathbf{k}}(w_j) \quad (16b)$$

We denote the projected CF orbitals $\tilde{\phi}$ as defined in equation (7) above. By convention, the single particle Jastrow factors J_i are kept inside the function g_{F} so that $g_{\text{F}}(z_i; w_j)$ is actually a function of all of the z 's and w 's through the J 's.⁴⁴ The subscript F here has been chosen to indicate that these are paired composite Fermions. Note that in the above expressions \mathbf{k} may stand for a general set of orbital quantum numbers (this will be important for spherical geometry where the free wavefunctions are spherical harmonics rather than plane waves).

The $g_{\mathbf{k}}$'s defining the shape of the pair wavefunction are variational parameters, analogous to the usual u 's and v 's. These parameters must be optimized to obtain a good wavefunction, although the optimal solution will certainly depend on the layer separation d . We also note that the expression (16) can describe pairing in arbitrary pairing channels depending upon the choice of $g_{\mathbf{k}}$ and the basis set $\{\phi_{\mathbf{k}}\}$. As a general

definition, when the pair wavefunction has the short distance form

$$g(z_i; w_j) \propto (z_i - w_j)^l h(z_i - w_j); \quad (17)$$

with $h(0) \neq 0$, we say this is l -wave pairing. However, note that $g(z; w)$ should asymptotically approach zero for $|z - w| \rightarrow \infty$, such that the pair wavefunction can be normalized. We also frequently use the atomic physics nomenclature where $l = 0$ is termed s -wave, $l = 1$ is the p -wave, and so forth. Furthermore, $l = +1$ is denoted as $p_x + ip_y$ pairing, whereas $l = -1$ is $p_x - ip_y$ pairing. (Unfortunately, in the literature “ $p_x + ip_y$ ” is used to denote either chirality). Note that the pairing symmetry is independent of whether we move the J^{zz} and J^{ww} factors inside or outside of the function g .

The choice of the pairing channel l affects the precise value of the flux $N_\phi = 2(N - 1) + l$ at which the trial state (16) occurs. For systems with finite N , we can thus distinguish the different possible pairing channels by studying the flux N_ϕ for which the groundstate of the system is incompressible as a function of system size N . Such a study has been undertaken in depth in Ref. 13 and it was found clearly that $p_x + ip_y$ pairing is supported by the numerical data. As the effective interaction of composite fermions derives from the interaction of the underlying electrons in a non-trivial manner, the pairing channel realized in the bilayer system was not reliably predicted by various theoretical approaches.^{3,11,31}

A case of particular interest is when the variational parameters $g_{\mathbf{k}}$ are defined as follows:

$$g_{\mathbf{k}} = \begin{cases} \text{anything nonzero;} & \mathbf{k} = \mathbf{k}_F \\ 0; & \text{otherwise} \end{cases} \quad (18)$$

It is easy to show that this choice of variational parameters recovers the product state of two composite fermion liquids (Eq. 8).

C. 111-state

When the spacing between the two layers becomes small, the bilayer system forms an interlayer coherent state. A number of different approaches have been used to understand this state and a large amount of progress has been made using a mapping to an iso-spin easy-plane ferromagnet.^{29,47} In this work, however, we will follow the Laughlin approach of considering trial wavefunctions in a first quantized description. When the distance between the two layers becomes zero, the exact ground state wavefunction of $\nu = \frac{1}{2} + \frac{1}{2}$ is known to be the so-called 111-state^{29,48}

$$\Psi_{111} = \prod_{i < j} (z_i - z_j) \prod_{k < l} (w_k - w_l) \prod_{r,s} (z_r - w_s); \quad (19)$$

where again we use z to represent particles in the upper layer and w to represent particles in the lower layer. In contrast to the CF state, (19) contains only one Jastrow factor between particles in the same layer so that the wavefunction is properly antisymmetric under exchange of particles in the same layer.

Thus, no additional determinant is needed to fix the symmetry as was the case in the CF state. In addition, (19) includes a Jastrow factor between particles in opposite layers. Consequently, there is no amplitude for finding two particles at the same position in opposite layers. This can be interpreted as each particle being bound to a hole in the neighboring layer. One can say the 111-state is composed of interlayer excitons.⁴ Another terminology is the Chern-Simons language where the electrons are transformed into bosons bound to flux quanta, where each flux quantum penetrates both layers. These “composite bosons” can be thought of as an electron bound to a vortex of the wavefunction in each layer. Condensing these bosons gives the wavefunction $\Psi_{\text{CB}} = 1$ for the composite particles and the transform back to an electron wavefunction (by reattaching the Jastrow factors) yields (19).

However, it is also useful to rewrite the 111 wavefunction using the Cauchy identity

$$\prod_{i < j} (z_i - z_j) \prod_{i < j} (w_i - w_j) = \prod_{ij} (z_i - w_j) \det \frac{1}{z_i - w_j} \quad (20)$$

which yields

$$\Psi_{111} = \det \frac{1}{z_i - w_j} \prod_{ij} (z_i - w_j)^2; \quad (21)$$

This notation resembles the form of a general paired bilayer state as discussed above in section II B. This resemblance has been noted previously,^{11,49} and from the form of the $1 = (z_i - w_j)$ factor, it has been concluded that the pairing symmetry is $(p_x - ip_y)$.¹¹ Here, we would like to propose a different interpretation. Since the Jastrow factors outside the determinant cancel the apparent singularity in Eq. 21, the phase obtained by taking an electron around its partner is actually $+2\pi$ rather than -2π . In fact, for the 111 state it is clear from the explicit form (19) that as any electron is taken around another electron in either layer, one accumulates a phase of precisely $+2\pi$. For clarity, it is useful to move the Jastrow factors in Eq. 21 inside the determinant. We obtain

$$\Psi_{111} = \det [g_{\text{B}}(z_i; w_j)] \quad (22)$$

where

$$g_{\text{B}}(z_i; w_j) = \frac{J_i^{zw} J_j^{wz}}{z_i - w_j} \quad (23)$$

and the interlayer partial Jastrow factors are defined by

$$J_i^{zw} = \prod_k (z_i - w_k) \quad (24a)$$

$$J_i^{wz} = \prod_k (w_i - z_k); \quad (24b)$$

Here, the subscript B means that we have a pairing wavefunction for composite **B**osons. This form suggests more that $g_{\text{B}}(z_i; w_j)$ represents pairing of $p_x + ip_y$ type since a phase of $+2\pi$ is obtained when z_i moves around w_j rather than -2π . As suggested by Ref. 11, it seems natural to have the same

pairing symmetry for $d > \nu_B$ and $d < \nu_B$. This then suggests that the relevant pairing symmetry for the composite fermions is $p_x + ip_y$ rather than $p_x - ip_y$. We emphasize that it is mostly just a matter of nomenclature whether we label the 111 state as having $p_x + ip_y$ symmetry or $p_x - ip_y$ symmetry. This ambiguity is a reflection of the fact that one can attach Jastrow factors to electrons to construct new particles. Depending on how the Jastrow factors are attached, the pairing can appear either $p_x + ip_y$ or $p_x - ip_y$. What is crucial, however, is that the wavefunction always picks up a phase of $+2\pi$ when z_i moves around w_j — a behavior identical to that of the $p_x + ip_y$ paired CF phase. This similarity of the 111 phase and the $p_x + ip_y$ paired CF phase is crucial in the next section.

D. Mixed CF-CB state

In section II B, we establish the general expression for an interlayer-paired CF state in the bilayer (16) which we believe should yield appropriate ground state wavefunctions for large $d = \nu_0$. Furthermore, in section II C we determine a way to write the 111 (CB) state, which is exact at vanishingly small $d = \nu_0$, as a paired state. Both these types of wavefunctions can be written as determinants of pairing functions g_F and g_B , respectively. Now, following the ideas of Ref. 34, we consider transitional wavefunctions that include both the physics of the CFs and the physics of the CBs. We propose the following extremely simple generalized form

$$\Psi^{\text{CF-CB}} = \det [G(z_i; w_j)] \quad (25a)$$

with

$$G(z_i; w_j) = g_F(z_i; w_j; \{g_k\}) + c_B g_B(z_i; w_j); \quad (25b)$$

where c_B is an additional variational parameter representing the relative number of CBs versus CFs. Note that as above, g_F is a function of the variational parameters $\{g_k\}$ which describe the shape of the pairing wavefunction.

In section III and Appendix A we will translate these wavefunctions onto the spherical geometry for which we have performed detailed numerics.

To elucidate the meaning of this linear interpolation between composite fermion and composite boson pairing functions, it is useful to consider more carefully the physics of the fermion pairing described by Eq. 16. Each entry in the matrix $g_F(z_i; w_j)$ is a sum of many terms (See Eq. 16b) with each term representing the filling of particles z_i and w_j into a particular pair of CF orbitals (one in each layer). Upon multiplying out the entire determinant, each term will include precisely N occupied CF orbitals, and as required by Pauli exclusion, no orbital may be occupied more than once. Terms with double occupation of the same orbital cancel out by antisymmetry of the determinant, even for non-orthogonal basis functions ϕ_i . The amplitude that a particular orbital is occupied is determined by the coefficients g_k (Compare Eq. 11). Now, let us consider instead the pairing function $G(z_i; w_j)$ which has both the fermionic g_F terms as well as the bosonic g_B terms (See Eq. 25b). When we calculate the determinant in Eq. 25a, each

$G(z_i; w_j)$ will be the sum of a term where the CB orbitals are filled for particles z_i and w_j (the g_B terms) and several terms where z_i and w_j instead fill a pair of CF orbitals. When we multiply out the entire determinant it results in a linear combination of all possible choices of filling M CF orbitals and $N - M$ CB orbitals. As with the case for the paired CF wavefunction, the amplitude of different orbitals being filled is determined by the coefficients g_k for the fermions and c_B for the bosons.

With this reasoning, we can actually reconstruct the mixed CB-CF wavefunctions from Ref. 34 as a special case of Eq. 25. To this end, let us fix c_B to some constant value, e.g. $c_B = 1$, and for all other variational parameters g_k let us use a step function (analogous to Eq. 18 where we represented the filled Fermi sea as a paired state), but with a reduced Fermi-momentum $(k_F)_F$:

$$g_k = \begin{cases} \infty; & \mathbf{k} \leq (k_F)_F \\ 0; & \text{otherwise} \end{cases} \quad (26)$$

Where a very large g_k is chosen, the corresponding state is forced to be occupied (the resulting normalization suppresses anything that does not include the maximal possible number of g_k terms). Due to the Pauli exclusion principle, every CF state may be occupied only once, and consequently the particles remaining once the CF-sea is filled up to the reduced Fermi momentum $(k_F)_F$ can only occupy composite boson orbitals. The choice (26) results in the probability for a CF to occupy a state with $\mathbf{k} \leq (k_F)_F$ to be equal to unity, which corresponds to a filled shell configuration. This construction is “equal” to the mixed CF-CB construction from Ref. 34. (By “equal” here we mean that the two constructions are equivalent up to the differences between projection prescriptions in the original Jain construction Eq. 3 and the Jain-Kamilla construction Eq. 6). In Appendix B, we show explicitly that the filled shell states among those analyzed in Ref. 34 can be reproduced accurately by choosing g_k as in Eq. 26.

It is very useful to remind the reader that both CFs and CBs could in principle experience effective magnetic (or Chern-Simons) fields due to their attachment to Jastrow factors. As in Ref. 34, we can write expressions for the effective magnetic field \mathcal{B}^σ seen by fermions (F) or bosons (B) in layer $\sigma = \text{F} \text{ or } \text{B}$ as

$$\mathcal{B}_F^\sigma = B - 2\phi_0 \rho_F^\sigma - \phi_0 \rho_B \quad (27)$$

$$\mathcal{B}_B^\sigma = B - \phi_0 \rho \quad (28)$$

where B is the external magnetic field, ϕ_0 is the flux quantum, $\rho = \rho^{\text{F}} + \rho^{\text{B}}$ is the total density in both layers combined, ρ_F^σ is the density of CFs in layer σ and $\rho_B = \rho_B^{\text{F}} + \rho_B^{\text{B}}$ is the density of CBs in both layers combined. It is important to note that precisely at $\nu = 1/2 + 1/2$, independent of the relative densities of CBs and CFs (so long as it is symmetric between layers), at mean-field level, both species experience zero total magnetic field. For the mixed CF-CB state with CF pairing, the number of CFs present may be uncertain. As mentioned above in the introduction, a pair of CFs in opposite layers can transform into a pair of CBs in opposite layers. It is easy to

see from Eqs. 27 and 28 that this process leaves the effective field seen by all species unchanged.

In contrast to the formula for the mixed fluid states given in Ref. 34, the present form (Eq. 25) with g_k according to Eq. 26 allows for an efficient numerical calculation. In our present approach, as explained below, the antisymmetry of the wavefunction is a natural result of the determinant (requiring $\propto N_1^3$ numerical operations), whereas the wavefunctions from Ref. 34 require explicit antisymmetrization, an operation that requires much computation power with an operation count scaling exponentially with the system size.

We emphasize again that while Ref. 34 considered a limited family of wavefunctions without CF pairing, the current approach (Eq. 25) allows for the handling of both nontrivial CF pairing and CF-CB mixtures simultaneously.

We now focus upon the question of whether, or under which circumstances, Eq. 25 is a valid lowest Landau level wavefunction. First, to test the requirement of antisymmetry, consider the interchange of 2 particles in the same layer, e.g. $z_i \leftrightarrow z_j$, thus in all columns k :

$$\begin{aligned} g_B(z_i; w_k) &\leftrightarrow g_B(z_j; w_k); \text{ rows } i; j \\ g_B(z_l; w_k) &! g_B(z_l; w_k); \text{ 8 rows } l \neq fi; jg \end{aligned} \quad (29a)$$

$$\begin{aligned} g_F(z_i; w_k) &\leftrightarrow g_F(z_j; w_k); \text{ rows } i; j \\ g_F(z_l; w_k) &! g_F(z_l; w_k); \text{ 8 rows } l \neq fi; jg \end{aligned} \quad (29b)$$

In other words, exchanging two particles amounts to interchanging two rows of the matrix $(G)_{ij}$.

The second condition to be checked is whether the proposed wavefunction is properly homogeneous, implying that it is an angular momentum eigenstate as required for the ground state of any rotationally invariant system. This condition is known to be true for both limiting cases — the 111 and the paired CF states. For it to remain true for the mixed CF-CB state, it is sufficient to require that $(g_F)_{ij}$ and $(g_B)_{ij}$ be of identical order in all variables. To check this it is sufficient to count the order (or number of zeros) that occur for a given variable in g_{ij} . For example, let us choose to look at the variable z_1 . For $i \neq 1$ we have $g_B(z_i; w_j) = J_i^{zw} J_j^{wz} = (z_i - w_j)$. The variable z_1 occurs only inside of J_j^{wz} and occurs only once. Therefore, it is first order in z_1 . Similarly for $i \neq 1$, in $g_F(z_i; w_j) = g(z_i; w_j) J_i^{zz} J_j^{ww}$ the variable z_1 occurs only inside of J_i^{zz} and occurs only one time, so that it is also first order. Let us now look at the term $i = 1$. In this instance, we have $g_B(z_1; w_j) = J_1^{zw} J_j^{wz} = (z_1 - w_j)$ which has z_1 occurring N times in J_1^{zw} , once in J_j^{wz} and once in the denominator, resulting in a total order N . For $g_F(z_1; w_j) = g(z_1; w_j) J_1^{zz} J_j^{ww}$ there are $N - 1$ powers of z_1 in J_1^{zz} and additional l powers in $g(z_1; w_j)$ if we have l -wave pairing (See Eq. 17), giving a total number of powers of z_1 equal to $N - 1 + l$. Thus, in order for this to match the degree of $g_B(z_1; w_j)$, we must choose $l = +1$ or $p_x + ip_y$ pairing of the Fermions. It is clear that choosing any other pairing symmetry would result in a wavefunction that is nonhomogeneous (therefore not an angular momentum eigenstate) upon mixing fermions with bosons. While we cannot rule out some first order phase transition between some other pairing symmetry for the CFs and a coherent CB phase, it appears to us that $p_x + ip_y$ is the only symmetry compatible with

coexistence of CBs and CFs.

III. NUMERICAL RESULTS

In this section, we present a numerical study of the variational wavefunctions discussed previously. In particular we focus upon Eq. 25, which includes Eq. 14 as an important special case. As our trial wavefunctions are given as variational states, we first need to optimize the variational parameters $(g_k; c_B)$ to obtain the optimal trial state for each layer separation d . Given an explicit expression for a trial wavefunction at layer separation d , Monte-Carlo may be used to numerically evaluate observables such as the ground state energy, which we compare to similar results calculated using exact diagonalization methods. We also evaluate the overlap of the trial states (25) with the exact groundstate wavefunctions. We find that our trial wavefunctions provide extremely accurate representations of the exact ground states.

To avoid complications associated with system boundaries, except in section III D 3 below, we choose always to work with the spherical geometry⁵⁰ with a monopole of $N_\phi = 2q$ flux quanta at its center. We give each electron not only a positional coordinate, but also a layer index which may be either $\#$ or \cdot . N electrons are put on the surface of the sphere where half of them occupy each layer ($N = 2N_1 = 2N_\# = 2N_\cdot$). We assume the limit of no tunnelling between the two layers, therefore, these can be thought of as distinguishable electrons. We focus upon filling fraction $\nu = \frac{1}{2} + \frac{1}{2}$ which corresponds to $N_\phi = 2N_1 - 1 = N - 1$. This is precisely the flux at which the 111 state occurs. Note, however, that for a single layer the composite Fermion liquid state with no effective flux occurs at $N_\phi = 2(N_1 - 1)$, which differs from what we consider by a single flux quantum. This difference in ‘‘shift’’ means that we are actually considering a crossover from the 111 state to a Fermi liquid state with one additional flux quantum. It turns out that this one additional flux quantum is appropriate here since precisely such a shift is induced by the $l = +1$ nature of the p -wave pairing (that we determined as the appropriate pairing channel in an earlier publication¹³).

On the sphere, the explicit form of the trial wavefunctions (25) is defined by the expansion of the pair wavefunction (16b), where the basis functions ϕ_k become the monopole harmonics $Y_{q\gamma m}$, with $q = \frac{1}{2}$ corresponding to p -wave pairing, as explained in detail in Appendix A.

The interaction between electrons is taken to be the Coulomb potential

$$V_{\#\#}(r) = V_{\cdot\cdot}(r) = e^2 [\epsilon r]^{-1} \quad (30)$$

$$V_{\#\cdot}(r) = V_{\cdot\#}(r) = e^2 \frac{h p}{\epsilon} \frac{1}{r^2 + d^2} \quad (31)$$

where r is the chord distance between the electrons, ϵ is a dielectric constant, and d represents the distance between the layers (measured in units of the magnetic length λ_D). Note that for simplicity, finite well width is not taken into account.

Since our Hamiltonian is rotationally symmetric on the sphere, we can decompose all states into angular momentum eigenstates. Our exact diagonalization calculations determine

ν	N	N_ϕ	$D(L=0)$	E_{trial}	$E_G \approx E_G$	$\langle \Psi_{\text{trial}} \Psi_G \rangle^2$
$\frac{1}{2} + \frac{1}{2}$	5+5	9	29 +9	$< 1.4 \cdot 10^{-3}$	> 0.984 (4)	> 0.984 (4)
	6+6	11	97 + 155	$< 1.9 \cdot 10^{-3}$	> 0.978 (4)	> 0.978 (4)
	7+7	13	884 +715	$< 2.2 \cdot 10^{-3}$	> 0.965 (9)	> 0.965 (9)
$\frac{1}{3}$	6	15	6	$5 \cdot 10^{-4}$		0.99289
	7	18	10	$5 \cdot 10^{-4}$		0.99273
	8	21	31	$5 \cdot 10^{-4}$		0.99082
	9	24	84	$5 \cdot 10^{-4}$		0.98816
	10	27	319	$6 \cdot 10^{-4}$		0.984 (3)
	11	30	1160	$7 \cdot 10^{-4}$		0.984 (2)
$\frac{2}{3}$	8	16	8	$4 \cdot 10^{-5}$		0.9987(2)
	10	21	52	$2 \cdot 10^{-4}$		0.9955 (7)
	12	26	418	$2 \cdot 10^{-4}$		0.994 (2)

TABLE I: Hilbert space dimensions of the $L = 0$ subspace for the examined bilayer systems and several reference states. For bilayer states two values are indicated corresponding to the fraction of states with odd and even parity under layer exchange. The respective subspace containing the ground state is typeset in bold. Data on the exact energies of single layer states was collected from [51]. The last column indicates overlaps of the respectively appropriate trial wavefunctions with the exact ground states (data from Ref. 52 or from our calculations, where errors are indicated).

the ground state to be in the angular momentum $L = 0$ sector. The trial ground state wavefunctions are also $L = 0$. In addition to rotational symmetry, the Hamiltonian exhibits a symmetry under exchange of the two layers. The ground state is found in the subspace with parity $(-1)^N$. Again, it is simple to check that this is also the symmetry of our trial wavefunctions.

Exact diagonalization calculations are performed here for system sizes of $N = 10, 12$ and 14 electrons for a large range of values of the interlayer spacings d . In order to evaluate the significance of our results it is useful to examine the size of the Hilbert space in which the Hamiltonian resides. While the full Hilbert space is very large (even for 10 electrons), once the space is reduced to states of $L = 0$, the space is significantly smaller. In Table I we show the dimensions of the $L = 0$ Hilbert space (and the dimensions of the even and odd parity parts of that space) for the different size systems. While these sizes may appear small we note that they are typical sizes for $L = 0$ subspaces for what are considered to be relatively large exact diagonalizations. For comparison in Table I we show the dimensions of the $L = 0$ spaces for a number of other typical quantum Hall calculations in the literature.

For a given interlayer spacing d , we first perform exact diagonalization to find the ground state, and then determine how “close” we can get to this state with a variational wavefunction. The variational wavefunction is a function of the parameters $\{g_{\mathbf{k}}\}$ (for both Eq. 25 and Eq. 14) and one additional parameter c_B (which we can think of as being set to zero in Eq. 14). While it is clear that with enough variational parameters one can fit any result, the actual number of variational parameters we use is quite small. First of all $g_{\mathbf{k}}$ can be assumed to be a function of $|\mathbf{k}|$ only. More accurately, on the sphere the orbital states are indexed by the quantum numbers n (the shell

index) and m (the z component of the angular momentum in the shell), and by rotational invariance of the ground state we can assume that the variational parameters are independent of m (as detailed in Appendix A). In other words, there is a single parameter per composite fermion shell (or composite fermion Landau level); we label these parameters as g_n . For the system sizes available in our exact diagonalizations, no more than 5 such variational parameters are necessary to obtain satisfactory trial states. Considering the dimensions of the symmetry reduced Hilbert space (shown in Table I) which is much larger than 5, we conclude that the agreement of our states with the exact ground state is nontrivial.

There are several ways to evaluate the quality of a given trial wavefunction (or the “closeness” of a trial wavefunction to an exact wavefunction). For example, one could compare the energy of the trial wavefunction to that of the exact ground state energy. By the variational principle, if one obtains the exact ground state energy, then the trial wavefunction must be the exact ground state. Another well-known measure of the quality of a trial wavefunction is the overlap of the trial wavefunctions with the exact ground state. We shall adopt these two measures of accuracy for the analysis in the main text of the current paper.

The details of the optimization methods used to obtain the right variational parameters for a good trial state at a given layer separation d are explained in Appendix C. In brief, however, we proceed as follows. If we optimize for the ground state energy E , a Monte-Carlo estimate of the Hamiltonian operator $\hat{H}(d)$ is obtained in a very restricted basis of states defined by the trial wavefunction Ψ_0 to be studied, and an initial guess of variational parameters $\gamma = \{c_B; g_0; g_1; \dots\}$. This basis is spanned by Ψ_0 and its derivatives $\Psi_n = \partial \Psi_0 / \partial g_n$ with respect to g_n . Diagonalizing the estimator $\hat{H}(d)$ yields a new set of variational parameters, which are used as an improved guess of γ . This procedure is iterated until convergence is reached. If we optimize for the overlap with the exact ground state wavefunction, the procedure is simpler as we can directly evaluate the gradient of the overlap $\partial = (\partial \gamma_i) \langle \Psi_{\text{trial}} | \Psi_{\text{exact}} \rangle^2$. Updating γ according to a steepest descent algorithm has proven sufficient to optimize the overlap. For further details, please refer to Appendix C.

In addition to the energy and the overlap with the exact ground state, one could compare the pair correlation functions (both inter-layer and intra-layer) of the trial wavefunction to that of the exact ground state. Since, for pairwise interactions, the pair correlation function completely determines the energy of the system, again, a trial wavefunction that has the exact ground pair correlation function must identically be the correct ground state. Such a comparison of correlation functions is given in Appendix D.

For very large system sizes of course we are unable to perform exact diagonalization. Nonetheless, we are still able to study this system by Monte-Carlo. In such cases, the variational parameters are optimized by simply attempting to minimize the energy of the trial state (as discussed in Appendix C), though we are uncertain of the proximity of the results to the exact ground state. At present, this possibility has not yet been fully exploited, and we limit our study of bigger systems

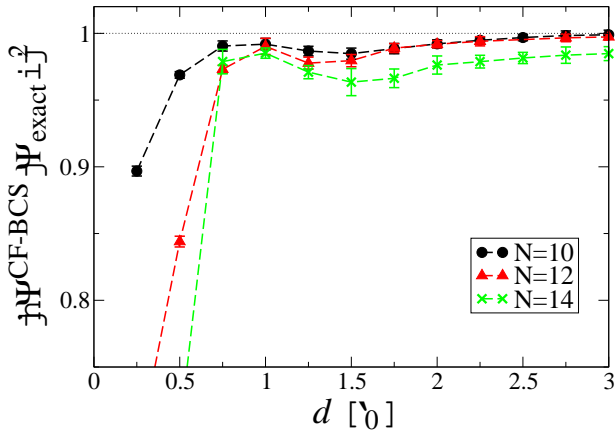


FIG. 1: Squared overlaps of $(p_x + ip_y)$ -wave paired CF trial states (Eq. 16) with the exact ground state, for $N = 5 + 5, 6 + 6$ and $7 + 7$. For $d \gg \gamma_0$ extremely high overlaps are obtained. However, for $d \sim \gamma_0$ the CF-BCS trial wavefunctions are not accurate, suggesting a phase transition around $d \sim \gamma_0$.

to filled shell states. This study is presented in Appendix B.

A. Paired CF results

In this section, we discuss the results for the paired CF wavefunctions (16) with pairing in the $p_x + ip_y$ channel. Figure 1 shows overlaps of our trial states with the exact ground state for several system sizes as a function of interlayer spacing. (This data has been previously presented in Ref. 13). In Figure 2, the relative errors of the trial state energies E_{trial} with respect to the ground state energy E_G are represented as $|E_{\text{trial}}(d; \mathbf{g}_n) - E_G(d)| / E_G(d)$ for two different system sizes of $N = 10$ and $N = 14$ particles. From these two figures, it is clear that the paired CF states yield excellent trial states for large d , whereas there is a layer separation d^{CB} below which the paired CF picture yields no good trial states. We find $d^{\text{CB}} \approx 0.9 \gamma_0$ and $d^{\text{CB}} \approx 1.1 \gamma_0$ for 10 and 14 particles respectively. For 12 electrons (not displayed), this value amounts to $d^{\text{CB}} \approx \gamma_0$ (See also Table II).

These results are surprising, since the regime where paired CF states yield very good trial states extends from infinite layer separation down to $d \sim \gamma_0$, well below the point where experiments observe the set-in of the various phenomena that are thought to be associated with spontaneous interlayer coherence and the presence of CBs or interlayer excitons. Given the large increase in d^{CB} between the systems with $N = 10$ and $N = 14$ particles, it is not clear at present how this extends to larger systems. A naive linear extrapolation with respect to the inverse system size N^{-1} based on the above values yields $d^{\text{CB}} \approx 1.76 \gamma_0$ in the thermodynamic limit, which is rather close to where a transition is observed experimentally.

Unfortunately extrapolation to the thermodynamic limit is made difficult by shell filling effects. In particular, $N = 12$ corresponds to having two CF shells filled in each layer (the lowest shell has two electrons per layer, and the next shell has

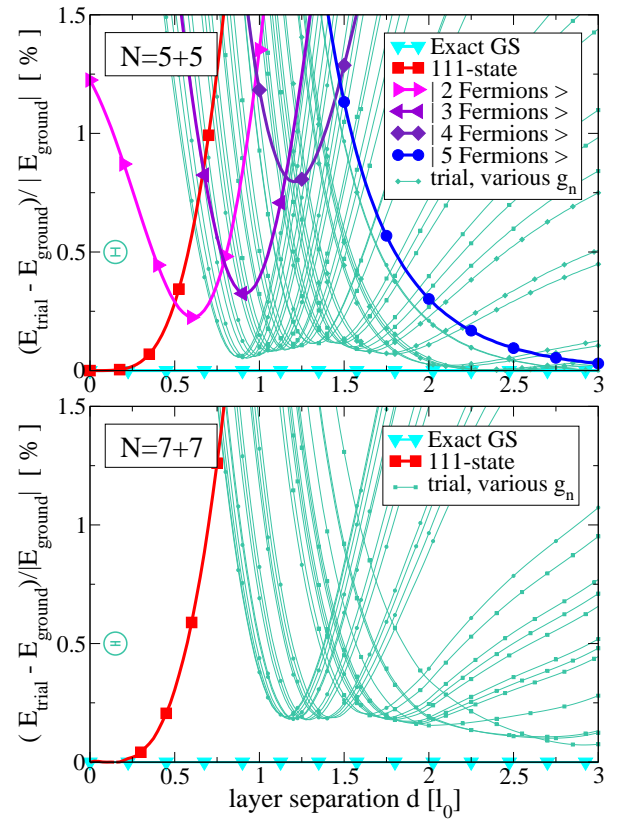


FIG. 2: Relative errors in energy of $(p_x + ip_y)$ -wave paired CF trial states (Eq. 16) in the bilayer for $N = 5 + 5$ particles (top) and $N = 7 + 7$ particles (bottom). Each of the represented curves corresponds to a different trial state, i.e. a different choice of parameters \mathbf{g}_n . The vertical axis is the fractional energy difference of the trial wavefunction energy with respect to the exact ground state energy $(E_{\text{trial}} - E_{\text{ground}}) / |E_{\text{ground}}|$. The largest errors are of order 1.4×10^{-3} and 2.2×10^{-3} for $N = 5 + 5$ and $N = 7 + 7$ respectively, when regarding only those layer separations greater than $d = d^{\text{CB}}$, where the paired CF Ansatz yields “good” trial states. The encircled error bar indicates the magnitude of Monte-Carlo error. For comparison, the mixed fluid trial states from Ref. 34 are represented as bold lines in the upper panel (see legend).

4 electrons per layer. See Appendix B). Thus, this particular system size could behave differently from the $N = 10$ ($N = 14$) case, where there is one CF-hole(electron) in the valence shell in each layer. Indeed, at large d , shell filling effects are quite strong, as was discussed in depth in Ref. 13. In particular, it was found that for large enough d , the system always follows Hund’s rule,⁵³ maximizing the angular momentum of the valence shell within each layer. Only for system sizes with filled shells (such as $N = 12$), or when there is a single electron or single hole in the valence shell in each layer (such as $N = 10$ and $N = 14$) can the Hund’s rule state be expressed as a CF-BCS wavefunction in the form of (16). For other cases, the large d limit of the CF-BCS states differs from the Hund’s rule state. However, as argued in Ref. 13, this Hund’s rule physics, involving only the N particles in the valence CF shell, should become less important as one goes to larger and

larger systems. If one assumes that the energy gain of pairing is roughly ΔN as is usual for BCS theory, then for any finite Δ , the pairing energy gain will always be larger than any putative Hund's rule energy gain in the thermodynamic limit.

In Ref. 13 arguments and detailed numerics were given supporting this picture: that for large d in the thermodynamic limit, the CF-BCS state prevails over the Hund's rule state. However, for very large d , with very weak coupling between the layers, no definite numerical conclusion could be reached. Nonetheless, whether or not one can draw conclusions about very large d , it is certainly the case that the numerics *strongly* suggested the existence of a CF-BCS phase for a range of intermediate d where the Hund's rule physics is not present.

For simplicity, in this paper, since we are concerned mostly with the physics at smaller d (and where an incompressible quantum liquid is observed), we will not address the Hund's rule physics further. To avoid this complication, we will focus on shell fillings such that Hund's rule is compatible with the CF-BCS state, so no competition arises. We refer the reader to Ref. 13 for further discussion of this issue.

B. Mixed CF-CB results

In order to obtain a complete description of the ground-state for small layer spacing d , we need to consider the mixed fluid description of the quantum Hall bilayer. Upon addition of CBs to the paired CF description, one obtains the family of mixed CF-CB states (Eq. 25). Technically this corresponds to adding one more variational parameter to the previously discussed case of paired CFs. Consequently, using this extended family of trial states yields at least as good results as with composite fermions only.

Numerical simulations confirm that the mixed fluid description of bilayer trial wavefunctions (Eq. 25) achieves an impressively precise description of the ground state for all d . This is borne out by the numerical results shown in Fig. 3 and Fig. 4, analogous to the above Figs. 1 and 2 except that now we have used the mixed fluid wavefunctions.

In Fig. 3 we find that over the entire range of d , the overlap with the exact ground state is extremely high for all systems sizes. The lowest overlaps occur at roughly $d = 1.5 \gamma_0$. As seen in Table I these "worst case" overlaps are comparable to the overlaps seen for the Laughlin $\nu = 1/3$ state for Hilbert spaces of similar size. Writing squared overlaps as $1 - \delta$, we find that the δ value for our worst trial wavefunctions are roughly twice that of the Laughlin state for similar Hilbert-spaces of comparable dimension. Similarly, in Fig. 4, we find that the largest relative error for the prediction of the ground-state energy occurs at intermediate distances close to $d = 1.5 \gamma_0$. These "worst case errors" are also listed in Table I. We find that the energy errors for our bilayer states are about 3-4 times as large as those of the Laughlin state at $\nu = 1/3$ for Hilbert-spaces of comparable dimension. Given that the Laughlin state is often referenced as a "gold-standard" for its accurate description of the exact ground state, we find the level of accuracy of our trial states to be quite satisfactory. (Note that the CF wavefunctions for $\nu = 2/5$ are even more accurate than the Laugh-

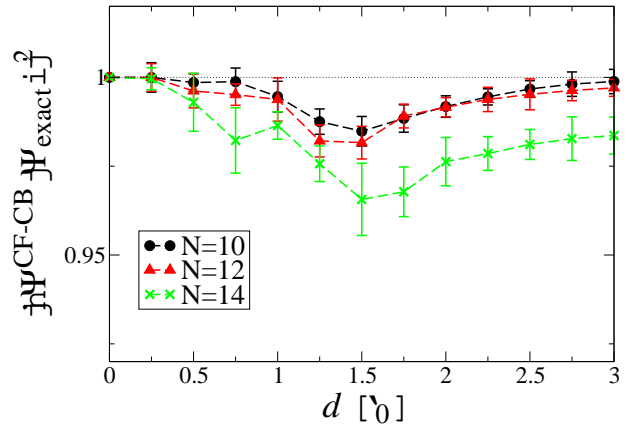


FIG. 3: Squared overlaps of the exact ground state with trial state for mixed CB-CF fluid with interlayer $(p_x + ip_y)$ -wave pairing. Over the entire range of d , extremely high overlaps are obtained. Data is shown for $N = 5 + 5$, $N = 6 + 6$ and $N = 7 + 7$. The quality of the overlaps are comparable to that of the Laughlin state, see Table I.

lin state at $\nu = 1/3$ for comparable Hilbert-space dimension). At layer separations d not too close to $1.5 \gamma_0$, the bilayer trial wavefunctions are even more accurate than the number quoted above, and may exceed the accuracy of the Laughlin and even of the $\nu = 2/5$ trial wavefunction.

For further comparison, in the upper frame of Fig. 4 are the energies (dark lines) of the mixed fluid wavefunctions first introduced in Ref. 34. As discussed above, these wavefunctions lack CF pairing that is included in Eqs. (16) and (25). Although these wavefunctions clearly capture some of the physics of the crossover from the 111 to the CF liquid, it is clear that pairing is required in order to have a high degree of accuracy.

Naturally, nearly exact trial states are obtained at $d \rightarrow 0$, where the appearance of CFs may be regarded as a perturbation of the 111-state (which is obtained by the particular choice of parameters $g_k = 0$ and $c_B = 1$, and which is the exact ground state at $d = 0$). However, the admixture of CFs becomes important at rather small d . We see that this admixture provides a nearly exact description of the fluctuations around the 111 state. However, in the regime of small layer separation, an equivalent description in terms of other excitations to the 111-state may be also suitable.^{5,54}

It should be noted that the number of variational parameters required to obtain good trial states becomes maximal at intermediate layer separations $d \approx 1.5 \gamma_0$. However, even at $d \approx 1.5 \gamma_0$, only four variational parameters are required for the system sizes we consider. In the limits of $d = 0$ and $d \rightarrow \infty$, writing the wavefunction in the form (Eq. 25) essentially amounts to rephrasing a parameterless trial state, respectively the 111-state and a product state of Fermi-liquids, in a different form (the case of $d \rightarrow \infty$ is slightly more complicated, as was discussed in detail in Ref. 13). As either regime is approached, the number of variational parameters required to describe the physics of the ground state decreases. For example, at $d \approx 0.5 \gamma_0$ and $d \approx 3 \gamma_0$ only two variational param-

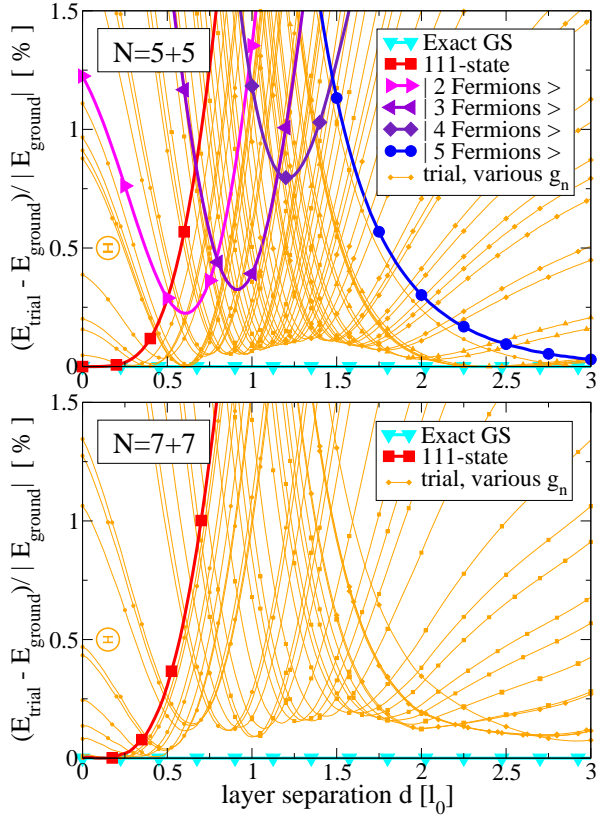


FIG. 4: Comparison of relative errors in energy for mixed CB-CF fluid with interlayer $(p_x + ip_y)$ -wave paired CF model systems with $N = 10$ (top) and $N = 14$ electrons (bottom). As in Fig. 2, each curve represents a different trial state. The mixed fluid states from Ref. 34 are highlighted in bold in the upper panel. Over the entire range of d , extremely good trial states are obtained, with a remaining error $\delta\epsilon < 2.2 \cdot 10^{-3}$. For intermediate d , where the states without pairing j Fermions i do not perform very well, considerable improvements are realized. Monte-Carlo errors are on the order of the encircled error bar.

ters are used.

It is at intermediate distances of $\nu_0 \cdot d \cdot 2\nu_0$ that the mixed fluid state is most different from both the 111-state and the CF liquid. In this regime, the influence of CF pairing is strongest, and the CFs tend to occupy orbitals in CF shells higher than the Fermi momentum of a filled CF Fermi sea (as shown in section III C, below). Although the overlap of our trial states has a minimum seen at $d = 1.5\nu_0$, which occurs in the regime that we identify as a paired state, we would like to point out that the magnitude of this overlap remains very high. In fact, the overlap is larger than that found for paired states in the single layer, i.e., for the Moore-Read state,³² or its generalizations for trial states in the weak-pairing phase at $\nu = 5=2$,⁵⁵ which is accepted to describe the physics of the quantum Hall state at that filling factor. Similarly, we conclude that CF pairing captures the essential physics of the quantum Hall bilayer system at filling factor $\nu = 1$ for intermediate layer separations d .

As a side note, we have confirmed numerically that the

mixed fluid trial states from Ref. 34 may be obtained in a manner prescribed in the approach to the filled shell cases. The general phenomenology that may be obtained from the analysis of filled CF shell states is discussed in Appendix B.

C. Occupation probabilities of CF shells

With the mixed fluid wavefunctions (Eq. 25), a vast family of trial states is available. Furthermore, the above results confirm that the mixed fluid wavefunctions allow for an accurate description of ground-state properties. As a step towards an understanding of the numerical results just presented, it is interesting to characterize the most successful trial states via the probability for an electron to occupy a given CF-LL within such a state.

In Figures 1-4, the various trial states were shown without specifying the explicit values of the variational parameters $\{g_n, g\}$.⁵⁶ Indeed, giving the precise values of these parameters may likely not have been very meaningful to the reader for two reasons. First, these parameters are defined only up to an overall global normalization. Secondly, and more importantly, the normalization of the individual composite fermion orbitals that the wavefunction is composed of is not well defined. If a basis of normalized single particle orbital is projected to the LLL using Eq. 7, we obtain a basis of many-body composite fermion orbitals that are no longer orthogonal, and which have lost their original normalization. In particular, the projected orbitals $\tilde{\phi}_i = \tilde{\phi}_i(z_1; \dots; z_N)$ become functions of all particles' coordinates. Their normalization \mathcal{N} could be defined by integrating out all coordinates but one. However, in such a definition, the normalization \mathcal{N} of a single orbital becomes ill defined, as it also depends on the correlations in the system, which however, are only known after a complete many-body state has been specified.

Since the normalization of the orbitals we use is ill defined,⁵⁷ we propose a universally applicable definition of the occupation $p(k)$ of a CF orbital $\tilde{\phi}_k$ with momentum k to be given by

$$p(k) = \frac{1}{2N} \frac{\partial \log \langle \Psi | \Psi \rangle}{\partial \log g_k}; \quad (32)$$

where $\Psi(g_k, g)$ is the bilayer wavefunction which is a function of the variational parameters g_k , and $\langle \cdot | \cdot \rangle$ denotes the unnormalized Monte-Carlo average. The relation (32) was successfully deployed for pairing in a single layer by two of the current authors,⁵⁵ and may be explained with the example of a simple one-particle two-state model with wavefunction $\Psi = g_1\phi_1 + g_2\phi_2$, which we allow to be unnormalized. Expanding the square of this wavefunction,

$$\langle \Psi | \Psi \rangle = \sum_{i,j=1,2} g_i g_j \langle \phi_i | \phi_j \rangle \quad (33)$$

we can see that Eq. (32) yields the proper occupation probabilities of both levels, provided that the overlap integral $\langle \phi_1 | \phi_2 \rangle$ vanishes. This is the case for the scalar product of wavefunctions in a regular orthogonal basis. This argument generalizes

to the many-body case simply by applying the product-rule for the derivative.

For the mixed bilayer states, however, we use the non-orthogonal basis of the LLL-projected CF orbitals. Nonetheless, we could verify that the occupation probabilities for states with filled CF shells (where we know the occupation probabilities (See Appendix B)) are obtained from (32) with very high accuracy, showing that the respective overlap integrals are small, thus giving a physical meaning to these occupation probabilities.

Surprisingly, applying Eq. 32 to the variational parameter for composite bosons c_B , does not yield the proper value for the occupation probability of the CB orbital. Consequently, we exploit the fact that this probability is complementary to the total occupation probability of the various CF orbitals. This allows to calculate the occupation probability of the CBs p_B as

$$p_B = 1 - \sum_n p(n); \quad (34)$$

where $p(n)$ is the probability to find an electron in CF shell n .

Let us now turn to the results obtained for the two selected systems sizes that we discussed in the previous sections. Taking the best trial state as a reference at each d , we may extract from our calculation the approximate separation-dependence of the occupation probability $p(n)$. The resulting data is displayed in Fig. 5.

We discuss these results going from right to left on the axis of layer separations. Upon looking at large layer separations, it is first noticed that the distribution at $d = 3\gamma_0$ is that of the CF Fermi sea. For example, in the lower panel for $N = 7 + 7$ electrons, the probability that an electron is in the lowest CF shell is $p(0) = 2/7 \approx 0.28$. For the next higher shell, which is fourfold degenerate, one finds $p(1) = 4/7 \approx 0.57$. The third shell accounts for the remaining probability. Upon going to intermediate layer separation, one notices the onset of pairing as one would expect by analogy with BCS theory: electrons are lifted above those orbitals within the equivalent of a Fermi-sea and occupy states at higher momentum, instead. Correspondingly, the occupations in the lowest two shells drop to allow the occupation of the higher ones ($n = 3$ included, which is occupied by a single electron per layer, initially). For $N = 5 + 5$, we follow an analogous trend of redistribution among the occupation of CF-levels, noting that the total probability of finding a particle in one of the excited orbitals is quite large, with absolute values close to 25%. Only at lower layer separation does the occupation of the CB orbital become important. Conversely, the occupation of CF orbitals plays an important role down to very low layer separations.

Now, the occupation of the CB orbital p_B shall be analyzed. At large layer separation, the value obtained from (34) drops slightly below zero. This is an inconsistency related to the empirical character of Eq. 32. However, the error is not very large, amounting to about 1%, which gives some confidence into our method, though it reminds us that it is approximate. We need to remark also, that the data is based on calculations for a restricted number of trial states, such that more substantial deviations are likely due to data that corresponds to not

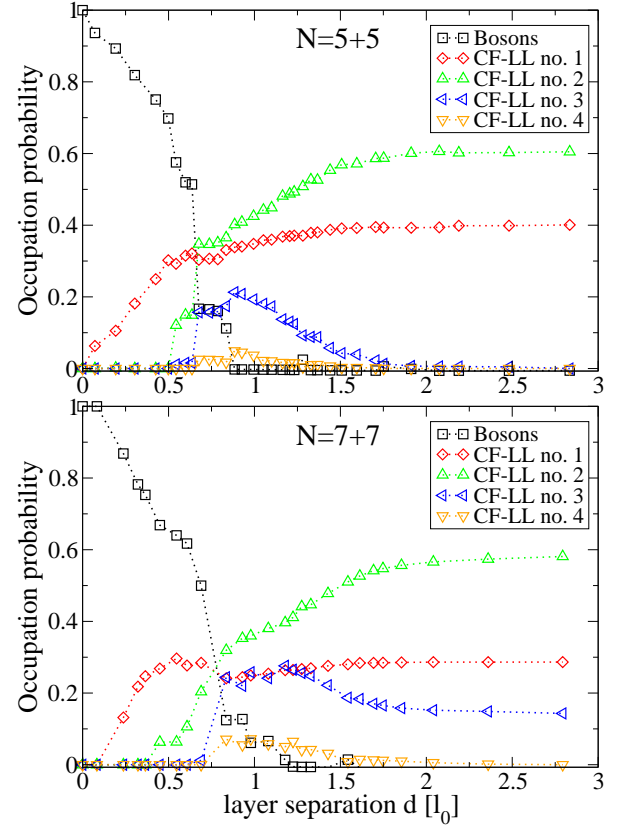


FIG. 5: Probabilities for a single electron to occupy a given orbital, as obtained from Eq. 32. A region of strong pairing, i.e. large probabilities to find an electron in an excited orbital above the would be Fermi-momentum, is found between $d \approx 0.8 \dots 1.5 \gamma_0$. Note that the probability p_B that an electron forms a CB (obtained as $p_B = 1 - \sum_n p(n)$) practically drops to zero, or slightly below, at $d \approx \gamma_0$. The kinks in the dependence of $p_B(d)$ are close to values which are related to the CF shell structure.

quite optimal trial states. The roughness of the curves illustrates this. Some of the features in the behavior of $p_B(d)$ might also be caused by filled shell (i.e., finite size) effects, given that kinks are featured at values close to $1 - n_s/N$ where n_s CFs yield a filled shell configuration.

D. Order Parameters

This section is devoted to discussing another means of characterizing the mixed fluid trial states — we discuss the broken symmetries of our wavefunctions and their associated order parameters. In the present case of the bilayer system with paired CF, two distinct symmetries, will be discussed in sections III D 1 and III D 2. In addition, we consider an additional topological order parameter of the paired CF system in section III D 3.

1. Excitonic Superfluid Order

In order to consider the first of the two potential symmetries of our quantum states, it is useful to employ the pseudospin picture. A density-balanced bilayer system has been described as a pseudospin field with its values confined to the x - y -plane.²⁹ In the ground state the orientation of this pseudospin field is homogeneous and (in the absence of interlayer tunneling) a spontaneous breaking of the $U(1)$ symmetry for rotations of the pseudospin around the z -axis occurs such as to select a preferred direction in the x - y -plane. The operator for the in-plane pseudospin thus yields a measure for detecting the symmetry of a coherent state in the bilayer system. In second quantized notation, this order parameter describes a flip of the pseudospin at position \mathbf{r} , noted as $\mathcal{F}(\mathbf{r})$:

$$\mathcal{F}(\mathbf{r}) = \Psi_n^\dagger(\mathbf{r})\Psi_\#(\mathbf{r}) \quad (35)$$

For the purpose of numerics at fixed particle number N_i per layer, the operator needs to be modified such as to conserve N_i . This is realized by taking the product $\mathcal{F}(\mathbf{r})\mathcal{F}^\dagger(\mathbf{r}^0)$ at two distant points \mathbf{r} and \mathbf{r}^0 which now preserves the number of particles in each layer. In the limit $|\mathbf{r} - \mathbf{r}^0| \rightarrow \infty$, one expects to recover the square of the expectation value of \mathcal{F} in a corresponding grand canonical ensemble. Thus we define

$$\mathcal{S} = \lim_{|\mathbf{r} - \mathbf{r}^0| \rightarrow \infty} \mathcal{F}(\mathbf{r})\mathcal{F}^\dagger(\mathbf{r}^0) \quad (36)$$

For a finite sized system, we must be content to move the positions \mathbf{r} and \mathbf{r}^0 as far apart as possible. One can visualize the action of this operator either as the associated pseudospin flips of two electrons in opposite layers at distant positions, or as the exchange of the real-space positions of these two particles. This operator can be easily calculated in our Monte-Carlo simulations carrying out this kind of exchange in position for pairs of electrons and monitoring the effect on the wavefunction.

For the 111-state, we have $\langle \mathcal{S} \rangle = 1$. Conversely, $\langle \mathcal{S} \rangle$ yields a very small value provided that the distance $|\mathbf{r} - \mathbf{r}^0|$ is chosen to be sufficiently large. Any finite geometry imposes a constraint on the limit in (36), but numerics confirm that $\langle \mathcal{S} \rangle \rightarrow 0$ to within roughly a part in 10^{-5} for accessible system sizes. As the sign of $\langle \mathcal{S} \rangle$ does not matter to distinguish the 111 and paired CF phases, we will refer to its absolute value

$$S = |\langle \mathcal{S} \rangle| \quad (37)$$

as the excitonic superfluid order parameter. Upon calculating S for mixed fluid states with filled CF-shells, we find that there is a monotonic relation between the order parameter S and the fraction of electrons $N_b = N$ that have undergone a CB-like flux attachment (See Appendix B). Furthermore, results for several different system sizes collapse on a single curve, such that we may estimate finite size effects to be small. We conclude that S is indeed a suitable order parameter for the transition between the CFL and the 111-state.

While it is true that increasing the fraction of CBs yields a larger order parameter, this is not the only factor influencing

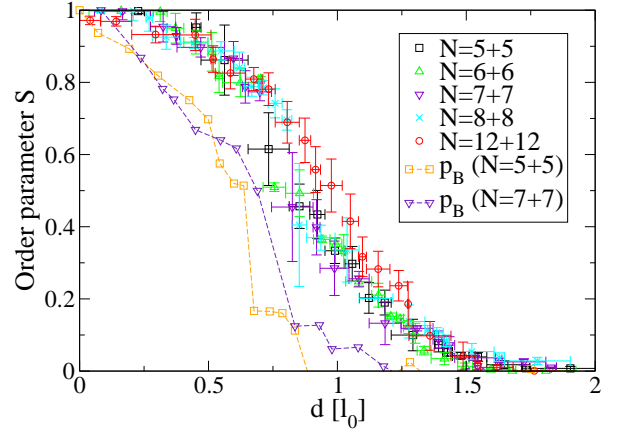


FIG. 6: A plot of the excitonic superfluid order parameter $S(d)$ for different system sizes according to the legend (symbols with error bars) and the fraction of bosons p_B as obtained from Eq. 32 (dashed lines). Data of system sizes $N = 8 + 8$ and $N = 12 + 12$ is based on a set of MC calculations with energy optimization (see Appendix C) and we have no according exact calculations available for comparison.

S . In particular, for our finite sized systems, nonzero values of the order parameter can be obtained for bilayer states within the paired CF picture, i.e. *without* composite bosons. Let us discuss this feature in detail by examining S calculated in our Monte-Carlo simulations for each of our trial states. We attribute the value obtained for the best trial state at a given d to represent the value S in the ground state at that d to a very good approximation. The data in Fig. 6 was obtained following this procedure. Error bars are established by taking into account the values of S for trial states, whose energies are within the range of Monte-Carlo errors from the best trial state.

A non-zero excitonic superfluid order parameter (i.e., S) for pure paired-CF states means that good trial states without adding composite bosons can be found above some layer separation d^{CB} which is well below the value d_c , where S becomes non-zero. While it is not easy to determine exactly the layer separation where mixed CB-CF fluid states become substantially better than the pure paired-CF states, it is more straightforward to estimate the paired CF states' maximal possible order parameter

$$S_{\max} = \max_{\mathbf{f}_{gk}g} \langle \Psi_{\mathbf{f}_{gk}g}^{\text{CF-BCS}} | \mathcal{S} | \Psi_{\mathbf{f}_{gk}g}^{\text{CF-BCS}} \rangle ; \quad (38)$$

where the maximization is over only paired CF states without any CBs. The fact that S can be nonzero without CBs is itself an intriguing phenomenon. For instance, considering $N = 5 + 5$ electrons, p -wave paired CF states yield a maximum S_{\max} as large as 42% the value of the CB condensate (the 111 state). Values for other system sizes are given in Table II. The numbers indicated for S_{\max} should be understood as estimates of a lower limit of this value. They were obtained by optimizing CF states for successively lower layer separations, until S ceased to increase.

$N=2$	4	5	6	7	8	∞
S_{\max}	0.64	0.42	0.38	0.30	0.20	< 0
d^{CB}	—	0.87 (3)	0.99 (4)	1.13 (5)	—	1.76 (11)

TABLE II: Scaling with system size of the maximal value of the non-zero excitonic superfluid order parameter for paired CF states S_{\max} in the absence of CBs. Pure paired CF trial states are relevant above the layer separation d^{CB} , as discussed in section IID. The last column indicates an (overly naive) linear extrapolation over N^{-1} to the thermodynamic limit.

This data, together with the values of d^{CB} discussed in section III A, sheds some light on the question of whether the paired CF state still has the symmetry of the 111-state in the thermodynamic limit. Given that the maximal value of the 111 order parameter decreases quickly with N as summarized in Table II, it seems that a non-zero S for paired CF states is a vestige of finite size systems. Roughly extrapolating d^{CB} in the same manner confirms this assumption, as it yields a value in the neighborhood of the onset of the excitonic superfluid order-parameter. Presumably, the order parameter should thus vanish in the thermodynamic limit for any state not involving composite bosons. On a more abstract level, one may reason that interlayer coherence is required for this order parameter to be non-zero. It seems unlikely that in the thermodynamic limit interlayer CF pairing alone would achieve this.

With these caveats, our theory supports a second-order transition between the excitonic superfluid (111 phase) and the paired CF state, as can be argued from the smooth variation of the order parameter. Furthermore, for all system sizes that we examined, we find approximately the same behavior of $S(d)$, which approaches zero at approximately $d = 1.5 \delta$. Again, we interpret the smooth tail of $S(d)$ found above this value of the layer separation as finite size effects and presume that the order parameter should approach zero at a precise value d_c in the thermodynamic limit.

In a recent DMRG-based numerical study,³⁰ it was shown that the character of the low-lying excited states changes at around $d = 1.2 \delta$ for a finite system with $N = 24$. In light of our results, this transition might correspond to the layer separation which separates states where CBs do or do not play a role. Note that the value predicted from extrapolation of our results is $d^{\text{CB}}(N = 24) = 1.3 \delta$.

2. CF Pairing Order

Assuming that the paired CF phase is distinct from the excitonic superfluid phase according to the above hypotheses, there should be a second order parameter that is particular to the paired CF phase. In analogy with BCS theory, one would expect an order parameter of the form $\langle \Psi_{\uparrow}(r) \Psi_{\downarrow}(r) \rangle$. However, here we consider pairing of composite fermions. The important difference is the Jastrow factors attached to the electrons contribute additional phase factors. Consequently, a guess for the order parameter proceeds by unwrapping these

phases to give

$$\exp \left[i \arg \left[\prod_k \langle z_k \rangle \right] \right] \exp \left[i \arg \left[\prod_k \langle w_k \rangle \right] \right] \Psi_{\uparrow}(z) \Psi_{\downarrow}(w); \quad (39)$$

where z and w encode the position r in the upper and lower layers respectively. However, pairing is in the p -wave channel and the order parameter is expected to have a phase that forces it to be zero at coinciding points $z = w$. A non-zero value might be obtained upon examining operators that are non-diagonal, i.e. $z \neq w$. Though, in such cases the order parameter continues to have a phase that makes numerical calculations difficult: averaging a vector rotating arbitrarily in the plane for different configurations gives a vanishing result. One must guess the proper phase of the order parameter. For example, $\exp \left[i \arg \left[\langle z - w \rangle \right] \right]$ would be appropriate for the p -wave case. Thus, we obtain

$$\begin{aligned} \mathcal{O}(z;w) = & \exp \left[i \arg \left[\prod_k \langle z_k \rangle \right] \right] \exp \left[i \arg \left[\prod_k \langle w_k \rangle \right] \right] \\ & \exp \left[i \arg \left[\langle z - w \rangle \right] \right] \Psi_{\uparrow}(z) \Psi_{\downarrow}(w); \end{aligned} \quad (40)$$

However, (40) still needs to be modified as numerics require an order parameter that conserves the particle number in each layer. In principle, one can multiply (40) by its hermitian conjugate invoking different positions $\mathcal{O}^{\dagger}(z^0;w^0)$ to obtain a candidate for an order parameter satisfying this requirement

$$\mathcal{P} = \mathcal{O}(z;w) \mathcal{O}^{\dagger}(z^0;w^0); \quad (41)$$

This is a rather complicated operator since it is a function of the four positions z, w, z^0 and w^0 . On the sphere, an additional difficulty arises as a magnetic monopole charge in the center of the sphere implies the presence of a Dirac string, i.e. a singular point where a flux tube penetrates the surface of the sphere in order to achieve magnetic flux conservation. This results in Aharonov-Bohm phases for wrapping around this point, which must be taken into account to define \mathcal{P} properly.

We have not yet succeeded to show that a suitably modified BCS order parameter has a non-zero expectation value for the paired CF states. However, given the nature of our construction of the wavefunction based on BCS theory, it seems likely that such an order parameter exists. We hope that in future work we will be able to demonstrate its existence explicitly.

3. Pairing Topology

The distinction between the excitonic superfluid phase and the paired CF phase should become very obvious on the torus (or periodic boundary condition) geometry where the chiral p -wave paired phase has a 4-fold topological ground state degeneracy^{11,58} whereas the 111 phase has a unique ground state, at least in the thermodynamic limit. One would expect that as d is decreased through the phase transition, the four-fold degeneracy should split, leaving a unique ground state at small d .

In figure 7 we show several energy spectra of exact diagonalizations⁵⁹ on the bilayer torus for different shaped unit cells and different (even) number of electrons. This data

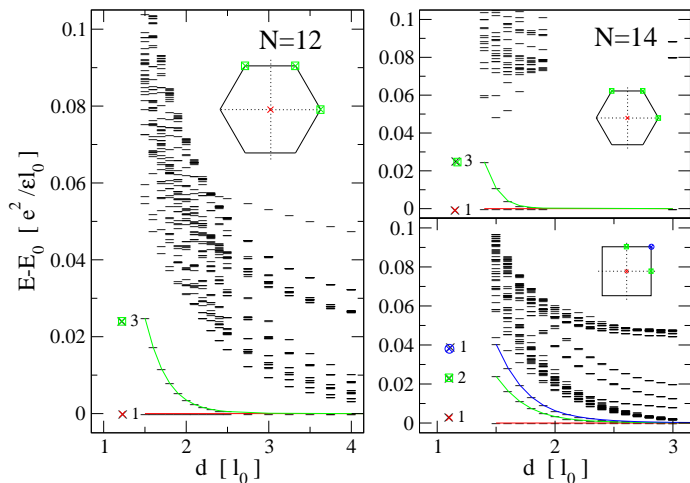


FIG. 7: We display the spectrum of the Coulomb Hamiltonian on the bilayer torus for different system sizes and geometries as a function of the layer separation d . The lefthand view shows $N = 6 + 6$ particles on a torus with hexagonal unit-cell, and the righthand view shows $N = 7 + 7$ particles in the hexagonal (top) and square (bottom) unit cells. The location in the Brillouin zone of the lowest four energy eigenstates is shown in the respective insets. The data is suggestive of an approximate fourfold degeneracy of these four lowest-lying states for intermediate d . Strong finite size effects are concluded from the marked difference of the spectra in the hexagonal and square unit cells for $N = 14$ particles, which precludes strong conclusions about the thermodynamic limit.

certainly suggests that the lowest four states are separated from the higher energy states by a clear gap, and at large enough d , these states become degenerate. Although suggestive, these data should be viewed with some caution. What one would like to see numerically is that at any d larger than a critical value, the four lowest energy states should become increasingly degenerate as the system becomes larger. However, this convergence (if present) is not easily seen numerically because of discrete shell filling effects. For example, in the case of the hexagonal lattice for $N = 14$, at $d = \infty$ the Fermi liquid state is already four-fold degenerate. Thus, for this system size and geometry, observation of a four-fold degeneracy should not be taken necessarily as evidence of pairing. Nonetheless, this data is suggestive that a phase exists with the topological order that is characteristic of pairing, i.e., having a fourfold groundstate degeneracy.

IV. DISCUSSION

Perhaps the most crucial question to be answered is the phase diagram at zero temperature with respect to variations of the layer spacing d . We know for certain that the 111 state is the ground state at very small d and that two noninteracting composite fermion Fermi liquids are the ground state for infinite d . We believe our work sheds substantial light on the intermediate values of d .

Our work (and also that previously presented in Ref. 13)

supports the notion that at large but finite values of d the system is in a $(p_x + ip_y)$ -wave paired state of composite fermions. It has been suggested in Refs. 3 and 12 that even for infinitely weak coupling between the layers there should be an instability to a paired phase. From our numerical work it is certainly not possible to determine if the transition to a paired phase occurs at finite or infinite d . However, it appears true in our work that the paired trial wavefunction is a notably better ground state than the unpaired wavefunction even at reasonably large values of $d \gg 2$. Since this appears true even when the inter-layer interaction is weak, and since this phase appears adiabatically connected to the Fermi liquid, we should conclude that this is a weak-pairing phase, rather than a strong pairing phase.⁵⁸ This conclusion is supported by the fact that, at least at $d > 1$, the occupancy of the orbitals with small (angular) momentum (i.e., the inner shells) is higher than the occupancy of orbitals with higher momentum (the outer shells) — this behavior is characteristic of a weak-pairing phase.⁵⁸ Finally, the conclusion of a weak pairing phase is supported by the topological degeneracies observed on the torus discussed in section III D 3 above.

At smaller distances between the layers, as discussed above, we found clear evidence of the order parameter (a broken $U(1)$ symmetry) associated with the 111, or excitonic superfluid phase. We analyzed this order parameter and found that it approaches zero smoothly at values close to $d = 1.5 \gamma_0$ with a tail at larger d attributed to finite size effects. This smooth behavior suggests a second order transition into the excitonic superfluid phase. Interestingly, we found that the order parameter can be nonzero even for our paired $p_x + ip_y$ CF-wavefunctions (with no additional CBs added to the wavefunction). Our current belief is that this is a finite size effect, and in the thermodynamic limit, this order parameter would become nonzero only when the wavefunction has a nonzero density of composite bosons. At small layer spacings where there is a finite value to the excitonic superfluid order parameter, we find that our wavefunctions with mixed CB-CF and with pairing of the CFs provide exceedingly good trial states. It is an interesting question, which we have not been able to fully answer, whether there is a distinct (pairing) order parameter associated with the CF-pairing in the presence of the condensed CBs.

There are a number of further issues which may be crucially relevant to experiment which we have not yet mentioned at all and we will now address briefly.

Finite Temperature and Low Energy Excitations: Our trial wavefunction approach is not particularly well suited to studies at finite temperature. Nonetheless, one could attempt to find trial wavefunctions for the low lying excited states which would then be thermally occupied at low but finite T . Certainly, the excitonic superfluid (111) phase as well as the $p_x + ip_y$ paired CF phase would have low energy Goldstone modes associated with superfluid counterflow (this is essentially a necessary result of having quantized Hall drag). Other excitations of these phases should be gapped, and would be less important at low T . At some higher characteristic temperature, the order parameters would be destroyed altogether. It is very possible, that the characteristic temperature for the paired

CF phase would be extremely low, particularly when the spacing between the layers is large. Like a superconductor, above this temperature, the putative paired CF system would behave like a CF-Fermi liquid with some additional (weak) correlations between the layers. Of course since this is a two dimensional system, vortex unbinding physics will be important and strictly speaking there is no long range order above zero temperature, and the transition from super to normal would be smeared to a crossover.

The picture of a mixed CF-CB fluid at small layer spacing discussed in this paper adds a number of possibilities to the finite T phase diagram. For example, one might imagine having a mixture of CFs and CBs where one or the other species is condensed (but not both). The case where the CFs are not condensed, but the CBs are condensed corresponds with the picture from Ref. 34 of a mixed CF-CB fluid where the CFs fill a Fermi sea, but do not pair (See Appendix B). Such a phase could have low energy excitations associated with excitations of the fermions around the Fermi surface. We note however that the phase remains incompressible with respect to “symmetric” density perturbations that change the total local charge in both layers.⁵⁴ To understand this incompressibility we simply note that when the total density compresses, the bosons would then feel an effective (Chern-Simons) magnetic field (See Eq. 28), which they can only accommodate by forming vortices — a gapped excitation. Another way to realize this is to note that motion of density of the entire system (both layers) remains subject to Kohn’s theorem and must only have an excitation at the cyclotron mode in the long wavelength limit.

Conversely, if one considers a density gain in one layer and a compensating density loss in the opposite layer, the bosons would feel no net field. Although such a density change would presumably pay the price of the capacitive energy between the two layers, at long wavelengths such a mode may still be low energy. Indeed, the superfluid Goldstone mode is of this form.

One might further ask whether there might be any novel low energy modes in the mixed CF-CB phase associated with motion of CFs in one direction and CBs in the opposite direction so as to preserve overall uniformity of charge. For example, we may consider the case where a current of CFs occurs in the same direction in both layers, such that $\rho_F'' = \rho_F^\#$ and $\rho_B'' = \rho_B^\#$ and the total density in each layer $\rho_B'' + \rho_F'' = \rho_B^\# + \rho_F^\#$ is a constant. In this case, there is no capacitive energy, and examining Eqs. 27 and 28 we see that there is no net field seen by the bosons, and there is no net field seen by the fermions. While naively it would appear that such a motion would yield very low energy modes, it is also possible that the pairing interaction would couple the motion of the bosons and the fermions, gapping such a mode even if the fermions are uncondensed.

Layer Imbalance: In principle our theory can be generalized to situations where there are unequal densities in the two layers. It is well known that the 111 wavefunction can easily accommodate layer imbalance.⁶⁰ In the paired-CF phase, on the other hand, this type of perturbation (like a Zeeman field in a traditional superconductor) is clearly pair breaking since the " and # Fermi surfaces would be of different sizes (Although in principle more exotic types of pairing could be con-

structed to accommodate such differences). A much more interesting question to ask is what happens in the regime where there are both CFs and CBs. The intermediate wavefunctions discussed in this paper (Eq. 25) do not appear to generalize obviously to cases where there are unequal numbers of particles in the two layers (as this would result in a determinant of a non-square matrix). We recall that in Ref. 34, mixed CF-CB wavefunctions were constructed which are identical to those discussed here (with no CF-pairing), where the antisymmetrization over all particles was done explicitly. There is no particular difficulty in generalizing that form to cases with layer imbalance, although such explicit antisymmetrization is difficult to handle numerically except in very small systems. Nonetheless, we can at least in principle consider such generalizations as trial wavefunctions, and we can further consider allowing pairing of the CFs. Because of the pairing interaction, one might guess that the CFs would be stabilized by having equal numbers of CFs in both layers (as discussed above), and that the density difference would be accommodated by moving CBs between the layers. The fact that experimentally, layer imbalance appears to stabilize the excitonic superfluid phase,²² suggests further that the transition to this phase coincides with the appearance of CBs.

Spin: In the experiments of Ref. 61 it has been suggested, that at least in certain samples, the system becomes spin polarized at low d but is partially polarized at larger d . The transition is thought to occur near the phase transition to the excitonic phase. Although all of the trial wavefunctions discussed here have been for fully polarized systems, they can certainly be generalized to nontrivial spin configurations. (One should not confuse the actual spin with the iso-spin, or layer index). For example, one could trivially consider having a Fermi sea with some spin down and some spin up CFs. Once one considers pairing of this (partially polarized) Fermi sea, there become many different possibilities,⁵⁸ some analogous to superfluid Helium 3. Other exotic possibilities could also occur. For example, one might imagine two Fermi seas, each pairing in the a p -wave channel. Or one could have unpolarized pairing in an s -wave channel. However, these exotic possibilities may not be experimentally relevant since the “superfluid” phase appears to be polarized,⁶¹ suggesting that, as the spacing between layers is reduced, an unpolarized Fermi sea condenses into a polarized state (possibly as a first order transition).

Tunneling: The wavefunctions we have constructed here are not only antisymmetric between electrons within a single layer, but are also antisymmetric between electrons in opposite layers. As such these wavefunctions are not particularly destabilized (or frustrated) by small amounts of interlayer tunneling that destroys the layer index as a good quantum number. One should expect, however, that tunneling between the two layers is quite suppressed for the CFs since the CF has to carry its Jastrow factor with it, thereby requiring relaxation of all of the surrounding particles. In other words, for a CF to tunnel, the entire correlation-hole complex needs to tunnel with it. (In yet another language, the effective magnetic fields in Eq. 27 are changed when a CF moves from one layer to another). In contrast, tunneling of CBs is expected to be

quite large, since the CB has an identical correlation hole in each layer. Indeed, once the CBs are at finite density, we have found that there is a nonzero expectation of the excitonic superfluid (111) order parameter which means essentially that it is uncertain which layer any CB is actually in and the zero bias tunneling is resonantly enhanced. With this consideration, we might expect that tunneling between the two layers will stabilize the CBs and destabilize the CFs. When there are CBs present, tunneling between the layers will also have the effect of gapping the Goldstone mode, since a particular phase relation is preferred between the two layers.

Transport: Several marked transport phenomena are observed in the bilayer systems.^{18,19,20,21,22,23} As discussed above, resonantly enhanced interlayer tunneling current is a signature of the excitonic superfluid (or 111) order parameter. In essence, a nonzero value of this order parameter indicates that in the ground state, each electron is superposed between two layers and therefore tunneling occurs very strongly, controlled by the relative phase between the two layers, analogous to the Josephson effect.

The other two dramatic transport observations are quantized Hall drag $\rho_{xy}^D = h/e^2$ and superfluid counterflow (which are very closely related to each other). In the interlayer-exciton superfluid (or 111) phase, both phenomena can be understood by the presence of composite bosons. One argues that superfluid counterflow derives from coherent transport of CBs or charge-neutral interlayer excitons. As these objects have no charge, they also do not couple to the magnetic field and generate no Hall voltage.⁴

The above reasoning is based on considerations regarding the CB condensate. Although our results show that the “pure” CB condensate or 111 state occurs only at layer spacing $d = 0$, we expect the transport features of this phase to remain qualitatively similar to those of the pure 111 state for any sufficiently small d where the excitonic order parameter (111) remains nonzero.³⁴

Crucially, we note that the two phenomena of quantized Hall drag and superfluid counterflow would also be observed in a $p_x + ip_y$ paired CF phase, identical to that of the 111 phase — although such a CF superconductor would be lacking the strong interlayer tunneling as discussed above. [The fact that such a p -wave superconductor shows quantized Hall drag and superfluid counterflow is easily derived using the technique of Ref. 58 (See also Ref. 11) to handle $(p_x + ip_y)$ -wave superconductivity, along with a Chern-Simons transformation to account for the fact that we are pairing composite fermions].

It might be interesting to study the Hall drag at interlayer separations just above the onset of interlayer tunneling. If experiments were to identify an intervening regime, which has quantized Hall drag, but no resonant tunneling, this would be an indicator of the $p_x + ip_y$ paired CF phase. Presumably one would want to examine this transition in high Zeeman field where no spin transition would complicate experiments. One should be cautioned, however, that our analysis of transport is very crude. A more accurate analysis would necessarily involve understanding the effects of disorder as well as possible edge mode transport, which has been completely neglected in this work.

V. CONCLUSION

In conclusion, we have derived a composite particle description for the ground state wavefunction of the quantum Hall bilayer system at filling factor $\nu = \frac{1}{2} + \frac{1}{2}$. This ground state is properly described by interlayer p -wave pairing of composite fermions above a layer separation d^{CB} . More precisely, this pairing instability occurs in the positive p -wave or $p_x + ip_y$ channel. Below d^{CB} , a mixed fluid phase with coexistence of composite bosons and composite fermions develops, and CBs successively replace paired CFs upon diminishing d . We should emphasize that positive p -wave pairing is the only pairing channel that is consistent with such a coexistence.

The precision of the composite particle description has the same order of magnitude as other important trial states in the literature of the quantum Hall effect, notably as the Laughlin-state at $\nu = \frac{1}{3}$. The agreement between the trial states and the exact ground state was checked using energies, overlaps and correlation functions, and was found to be in good agreement.

We analyzed the order parameter of the broken U(1) symmetry of the excitonic superfluid (the 111-state order parameter), and found it to approach zero smoothly at values close to $d = 1.5 \gamma_0$ with a tail attributed to finite size effects. We also found this order parameter to be non-zero for the pure paired-CF-phase. Though we cannot exclude the contrary with absolute certainty, we believe that this is a phenomenon occurring only in finite size systems. From the shape of the order parameter, we conclude that the phase transition between the 111-excitonic-superfluid phase and the paired CF phase is of second order. The precise value of the layer separation where this transition occurs cannot be inferred from our numerics, since the order parameter continues to be non-zero at all layer separations in small systems. The transition from the p -wave paired CF phase to an excitonic superfluid phase might also be roughly identified by the splitting of a 4 fold degeneracy on the torus, indicative of the paired CF phase — although our finite size torus data needs to be viewed with some caution.

Acknowledgments

The authors gratefully acknowledge helpful discussions with B. Halperin, N. Bonesteel, P. Lederer and N. R. Cooper. G.M. would like to thank N. Regnault for kind assistance with the DiagHam libraries. E.H.R. acknowledges support from DOE grant DE-FG03-02ER-45981. G.M. acknowledges support by EPSRC Grant No. GR/S61263/01.

APPENDIX A: PAIRED CF WAVEFUNCTIONS ON THE SPHERE

The geometry chosen for our numerical calculations is the sphere, which has the benefit of avoiding boundary effects for finite-size systems. For our purposes, the most suitable coord-

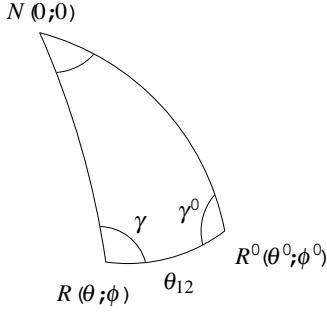


FIG. 8: Definition of the different angles for Eq. A5 taken from Ref. 65, adapted to our notations. Points R and R^0 indicate the positions of two electrons, and a third reference point can be chosen as the north pole N of the sphere. Generally, the reference point is given by the singular point of the section for a given representation of the monopole harmonics.⁶⁴

dinates are the spinor coordinates

$$u = \cos(\theta/2)e^{i\phi/2} \text{ and } v = \sin(\theta/2)e^{i\phi/2}: \quad (\text{A1})$$

In the following, it is convenient to change notations such as to write particle coordinates with two indices: the upper index indicates the pseudospin and designates the layer to which it belongs, whereas the lower index indicates the particle number. Thus, $(u_i^\sigma; v_i^\sigma) \in \mathbb{C}^2$ describes the location of particle i with pseudospin σ . The external magnetic field is represented by a magnetic monopole of strength N_ϕ in the center of the sphere, and it is useful to work in the Haldane gauge.⁵⁰ In particular, using the formalism of the stereographic projection between the plane and the sphere,⁶² one then obtains wavefunctions on the sphere which can be expressed entirely in terms of u 's and v 's and contain no additional phase factors. Our purposes require the translation of Jastrow factors to the new spinor coordinates on the sphere. A coordinate z translates to pseudospin up ($''$) and a coordinate w translates to pseudospin down ($\#$), e.g.,

$$(z_i \ w_k) \in (\Omega_i'' \ \Omega_k^\#) \quad (u_i'' \ v_k^\# \ u_k^\# \ v_i''): \quad (\text{A2})$$

Furthermore, the knowledge of a complete set of eigenstates ϕ_i is required to describe (16) on the sphere. These eigenstates are given by the monopole harmonics^{63,64,65} written as $Y_{q\ell m}$ for a total flux $N_\phi = 2q$, and the angular momentum quantum numbers $\ell = \ell_j \pm n$ and $\ell_j \geq |\ell|$. These orbitals are organized in a shell structure related to the Landau levels on the plane. The LL-index takes integer values $n = 0; 1; 2; \text{etc.}$ Contrarily to the plane, the degeneracy d_n of these ‘Landau levels’ is not constant but increasing with n as

$$d_n = 2(\ell_j \pm n) + 1: \quad (\text{A3})$$

In the thermodynamic limit, $q \rightarrow \infty$, whereas n remains finite, such that the constant LL-degeneracy of the plane is recovered.

The proper pair correlation function on the sphere might be deduced entirely from the requirements of its antisymmetry and the condition imposed on the flux-count for the resulting bilayer wave function (16) to be commensurable with

the 111-state. Nonetheless, let us discuss the symmetry of this two-point function (before projection to the LLL) in more general terms. A general pair wavefunction on the sphere may be expanded in terms of monopole harmonics, such that

$$g(\Omega_i''; \Omega_j^\#) = g(\Omega_i'' \ \Omega_j^\#) = \sum_n \sum_m g_{nm} Y_{\frac{1}{2}, \frac{1}{2} + n, m}(\Omega_i'') Y_{\frac{1}{2}, \frac{1}{2} + n, m}(\Omega_j^\#): \quad (\text{A4})$$

Here, the pair $(\mathbf{k}; \mathbf{k})$ has been replaced by its analogue on the sphere $[(\ell; m); (\ell; -m)]$. Rotational invariance of (A4) imposes that $g_{nm} = g_n$ independent of m . In the case of p -wave pairing, we must deal with a slightly more complicated case, since the pair correlation function is then not rotationally invariant, but rather acquires a phase. This is reflected by a less restrictive condition $g_{n, \ell_j - m} = g_n$. The angular behavior of (A4) may then be analyzed according to Eq. 25 from Ref. 65. This equation expresses the sum over the angular momentum quantum number m of a product of two monopole harmonics in terms of an amplitude depending solely upon their distance on the sphere, and a phase depending on several angles. For our purposes, we need to set $q = q^0$, and then take into account the relationship for the complex conjugation of the monopole harmonics, (Eq. 1 in Ref. 65) in order to deduce the relationship

$$\sum_m (1)^{\ell_j + m} Y_{q\ell m}(\theta; \phi) Y_{q\ell; m}(\theta; \phi) = \frac{2\ell + 1}{4\pi} Y_{q\ell; \ell}(\theta_{12}; 0) e^{iq(\phi + \phi^0)} e^{iq(\gamma - \gamma^0 + \pi)}: \quad (\text{A5})$$

This equation holds independently for each shell n . The angles $\phi; \phi^0; \gamma$ and γ^0 occurring in this expression are named according to our own conventions and indicated in Fig. 8. The third point of this triangle is a reference point, that is given by the singular point of the section on which the monopole harmonics are defined. The phase $\delta\phi$, accumulated when taking the two particles around each other with a small angular separation, may be deduced from the last term in (A5). For a half rotation (i.e. changing the position of both particles), both γ and γ^0 vary by π , but with different signs, whereas ϕ and ϕ^0 merely change roles. We then have $\delta\phi = 2\pi q$. Thus, pair wavefunctions expanded in monopole harmonics $Y_{q\ell m}$ correspond to $2q$ -wave pairing, following the analogy with (17). The choice of $q = \frac{1}{2}$ for the mixed fluid bilayer wavefunctions is consistent with the phase of the pair wavefunction found in the 111-state. Analogously, this may also be concluded from the flux-count argument introduced at the end of section IID: naturally, an orbital $Y_{q\ell m}$ adds a number $N_\phi = 2q$ flux to this count. Thus, with $q = \frac{1}{2}$, we recover the previous result that a mixed CF-CB fluid requires positive p -wave pairing of composite fermions.

To summarize, we have outlined how to write the mixed fluid wave function with paired CF on the sphere. Taking into account the above considerations, the explicit expression upon

adding the projection to the LLL⁴³ is:

$$\Psi^{\text{CF CB}} = \det \frac{J_i^{zw} J_j^{wz}}{u_i v_j} + \dots \quad (\text{A6})$$

$$J_i^{zz} J_j^{ww} \sum_{n,m} (1)^{q+m} g_n \tilde{Y}_{\frac{1}{2}; \frac{1}{2} + n, m}(\Omega_i) \tilde{Y}_{\frac{1}{2}; \frac{1}{2} + n; m}(\Omega_j) :$$

As a reminder, arguments (Ω_i^σ) denote the coordinates particle i with pseudospin σ . Jastrow factors must be expressed following the replacement rule (A2).

APPENDIX B: NUMERICAL RESULTS FOR MIXED CF-CB STATES WITH FILLED CF SHELLS

The analysis of the mixed fluid bilayer states with CF pairing presented in section III has shown that, in general, the ground state features non-trivial CF pairing. However, the precise shape of the pairing potential must be found by optimization over a small set of variational parameters. Since this requires a considerable numerical effort, it is interesting to analyze a particular subclass of the mixed fluid states: those with filled CF shells. Using the term ‘shells’, we refer to the spherical geometry, as discussed in Appendix A. These filled shell states are obtained following the choice of parameters (26) for the g_n , i.e. choosing very large coefficients up to a reduced Fermi momentum $(k_F)_F$ to force the respective number of electrons into CF orbitals. Remaining electrons then occupy CB states.

Given the degeneracy of CF shells on the sphere (A3), with $q = \frac{1}{2}$ for the mixed fluid states, there are a small number of possible filled shell states for each system size N . Explicitly, the series of possible CF numbers per layer for n_s filled CF shells is given by

$$N_{1F}(n_s) = n_s(n_s + 1) = 2;6;12;20; \dots \quad (\text{B1})$$

Though these filled shell states are known not to be ground states of the bilayer system, they represent intermediate states between the 111-state and the CFL, and are better approximations of the ground state than either of the latter two states for intermediate layer separations.

As an example, \mathfrak{Z} Fermions_i as described in Ref. 34 is such a filled shell state without CF pairing. In order to show that our calculation reproduces exactly the state \mathfrak{Z} Fermions_i for large g_0 , and $g_n = 0; 8n - 1$, we have calculated the overlap of that state with a special case of our trial states (with g_0 large and all other $g_n = 0$), and find it to be precisely equal to one within the numerical precision of our calculation: \mathfrak{Z} Fermions_i $\Psi^{\text{CF-CB}}(g_0; \infty) \int \dots = 0.9999999 \dots 10^6$, for an overlap integral evaluated with 5×10^6 Monte-Carlo samples.

The agreement we have found supports our claim that we can indeed generate precisely the mixed CF-CB states introduced in Ref. 34 using our single determinant wavefunctions. This agreement further supports our interpretation of the g_n as controlling the occupation probability of the respective CF shell. Note that when choosing g_n to be large, this means that

the respective CF states are inert (i.e., the orbitals are fully filled and they do not participate in nontrivial pairing). It then does not matter whether the pair correlation function is chosen symmetric or antisymmetric.

In the case of filled CF shells, one can argue that our paired CF description and the mixed fluid picture from Ref. 34 are identical. However, we also find perfect agreement for the state where all electrons occupy CF orbitals, \mathfrak{Z} Fermions_i, which is not a filled shell configuration: the overlap of the corresponding trial state with the explicitly constructed CFL state \mathfrak{Z} Fermions_i was found to be \mathfrak{Z} Fermions_i $\Psi^{\text{CF-CB}}(g_0; g_1; \infty) \int \dots = 0.999991 \dots 10^5$ (evaluated over 10^6 Monte-Carlo samples). As opposed to the previous case, in order to obtain this agreement, it is required that the pair correlation function g_F be chosen antisymmetric (see Appendix A). As pointed out in the main text, and discussed previously in Ref. 13, this agreement is possible only for cases where the CF-sea deviates from a filled shell configuration by at most one electron per layer.

Since the fraction of CFs and CBs is known for the mixed fluid states, these represent a testing ground for the validity of Eq. 32. Numerical evaluation indeed confirms that the correct fraction of CFs $p(n_s) = N_F(n_s) = N_1$ is obtained from (32) within about one percent error (See Table III). Typically, when calculating a Fermi liquid state, $\sum_{n_s} p(n_s)$ is slightly larger than one but remains within the same error margin.

Having clarified that the filled CF shell states represent a subclass of the mixed fluid states in Ref. 34 but with the advantage that the representation (A6) is computationally easier to evaluate, we may study this class of states up to very large system sizes.

We have studied larger systems, focusing our attention to system sizes of the sequence (B1). For a system size corresponding to n_s filled shells, we may construct $n_s + 1$ different trial states, notably the 111-state and the states with $1; 2; \dots; n_s$ filled shells. The state with all shells filled (i.e. the CF Fermi liquid) gives us a criterion to test whether the parameters g_n have been chosen large enough to transform all particles to composite fermions. Such a state features no interlayer correlations and, consequently, its interlayer correlation function should be constant. All one needs to do is to tune the g_n until this situation is reached. Empirically, we have found that values $g_n \approx 1000$ satisfy this criterion.

The biggest system analyzed in this way had $N = 42 + 42$ particles. As the exact ground state energy is not known for such large systems, we only compared the different filled shell states. At zero layer separation, the 111 state is the exact ground state. Interestingly, states with a small number of CFs have a very large overlap with the 111-state, such that MC simulations have difficulty in resolving their difference in energy. However, there is a general tendency that states including CFs have lower energy at increasing d . This suggests that a finite fraction of CF could eventually be favorable at any finite d in the thermodynamic limit. Going from small to larger layer separations, states with subsequently more filled CF-LLs clearly become the most favorable trial states.

The layer separations d_{n_s} , where we observed the level crossings between a first state with $n_s - 1$ filled CF shells

N_1	1 filled shell		2 filled shells				3 filled shells				$\delta [\sum p]$		
	$p(0)$	δp_0	$p(0)$	δp_0	$p(1)$	δp_1	$p(0)$	δp_0	$p(1)$	δp_1		$p(2)$	δp_2
5	0.400974	+0.24	0.400877	+0.22	0.604851	+0.81							+0.57
6	0.334152	+0.25	0.334157	+0.25	0.678183	+1.73							+1.23
7	0.286419	+0.25	0.286421	+0.25	0.581292	+1.73	0.285971	+0.09	0.575032	+0.63	0.142858	0.0	+0.94
8	0.250619	+0.25	0.250620	+0.25	0.508638	+1.73	0.250559	+0.22	0.500022	0.0	0.258746	+3.5	+0.93
12	0.167082	+0.25	0.167082	+0.25	0.339134	+1.74	0.167082	+0.25	0.339158	+1.75	0.522862	+4.57	+2.91

TABLE III: Occupations $p(n)$ calculated according to Eq. 32 for filled shell states. At a given system size $N_1 = N=2$, values for sample calculations of all possible filled shell states are indicated. The deviations of $p(n)$ from the expected occupation probabilities $\delta p_n = [p(n) - (N_{1F}(n)/N_1)] \cdot 100$ are indicated in percent. The last column gives the percent deviation from 1 for the sum of occupation probabilities of the state with the maximal number of filled shells.

and a second one with n_s shells filled are spread out over a large interval of layer separations ranging from $d_0 \approx 0.05 \gamma_0$ to $d_s \approx 1.5$. As stated before, neither of the filled shell states describes the ground state of the system at the point of their level crossing. Nonetheless, the d_{n_s} provide an estimate of the range of $N_F=N$ that would best characterize the ground state at this layer separation in the absence of CF-pairing. From this kind of reasoning, we can infer that

$$\frac{N_F(n_s - 1)}{N} \cdot \frac{N_F}{N} \cdot \frac{N_F(n_s)}{N} : \quad (\text{B2})$$

Collecting data from level crossings d_{n_s} at different system sizes, we established Fig. 9, where we have represented the complementary ratio of composite bosons $N_B=N - N_F=N$. For the filled shell states, the ratio $N_B=N$ is related to the order parameter $S = \langle \mathcal{N} \rangle$ via a monotonically growing function (See the inset of Fig. 9).

Given that CF pairing predominantly lowers the energy of states that contain a substantial fraction of CFs, the range for $N_B=N$ indicated in Fig. 9 should be seen as an estimate for the upper bound of the fraction of bosons. This is most drastically illustrated by the occupation probability of CB orbitals p_B (for $N = 5 + 5$ particles) that is given for reference in this figure. At small layer separations, where the mixed fluid description is at work, this curve is within the error bars deduced from the filled shell analysis. However, once the paired regime is approached, the true occupation of boson orbitals drops rapidly and the estimate made here clearly overestimates the actual value.

APPENDIX C: NUMERICAL METHODS

As stated in section III, the aim of our numerical simulations of the bilayer states (25) was to show that they potentially represent the ground state. However, to achieve an explicit representation of the ground state at a given layer separation d , one must find the corresponding set of variational parameters $\{g_n; c_B; d\} = \gamma$ that yields an optimal trial state (assuming a time reversal invariant interaction, all LLL wavefunctions can be written as polynomials with real coefficients, so $\{g_n; \gamma\}$ were considered real). This was realized either by maximizing the overlap with the exact ground state, or by

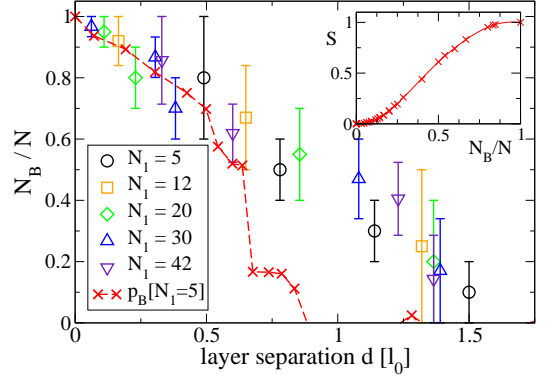


FIG. 9: Intersections of the energy levels of filled CF shell states allow deduction of estimates for the range of the most favorable fraction of CB at the layer separation d of the point of intersection. The results for various system sizes as small as $N_1 = 5$ and as large as $N_1 = 42$ electrons are represented collectively in this plot, and show a good coherence. Note that CF are formed in the system at very small d . A rough linear extrapolation of these results suggests that the ratio $N_B=N$ would vanish at approximately $d = 1.7 \gamma_0$. However, CF-pairing changes these figures, as highlighted by the occupation probability p_B for $N_1 = 5$ that is given for comparison. The inset shows the monotonic relationship between the order parameter S and the fraction of bosons for data from various filled shell states at different N .

minimizing the energy. Both operations represent non-trivial optimization problems.

In general, optimization algorithms require a large number of function evaluations before obtaining a good ‘guess’ of the optimal solution. Furthermore, our calculations were based upon Monte-Carlo simulations, a statistical method which yields statistical errors vanishing only as the inverse square root of the number of samples. This means that any optimization method is bound to make a trade-off between the uncertainty it allows for the precision of function evaluations and the number of such evaluations it requires.

Monte-Carlo sampling to evaluate expectation values is used in both methods below. Naïvely, each set $\gamma = \{g_n; c_B; d\}$ requires a separate Monte-Carlo simulation, though it is possible by using correlated sampling to simulate at the same time many choices of these parameters. A prerequisite for corre-

lated sampling is that correlations in the simulated wavefunctions are similar, such that the ensemble of samples used is similarly relevant to all of them. With this approach, it is easy, for example, to numerically evaluate local derivatives with respect to the variational parameters. Best results for our calculations were achieved by using a self-consistent sampling function F — an expression obtained as a Jastrow product form exploiting the correlation functions⁶⁶ $h_{\sigma\sigma}^{\gamma}$ calculated in the same run (let the superscript γ be a reference of a distinct trial state). This yields

$$F = \prod_{i<j} h_{nn}^{\gamma}(\zeta_i, \zeta_j) \prod_{i<j} h_{\#\#}^{\gamma}(w_i, w_j) \prod_{ij} h_{n\#}^{\gamma}(\zeta_i, w_j); \quad (C1)$$

where $h_{nn}(r) = h_{\#\#}(r)$ by symmetry. The most important part in this Ansatz are the interlayer correlations $h_{n\#}$, as the intralayer correlations are rather similar for *all* possible choices of the parameters γ .

1. Energy optimization

Due to the statistical errors that underly the Monte-Carlo simulations, computation time increases as the inverse square of the required precision, such that any optimization scheme using local derivatives of the energy is difficult. Iterative comparison of neighboring states in correlated sampling is a slow route to optimization. As the results shown in section III unveil, the difficulty of finding a good optimization scheme suitable for our case is also due to the inherently good correlations common to all trial functions: further improvement only concerns rather small relative differences in energy.

To meet these challenges, we successfully deployed a rather subtle optimization method⁶⁷ based on iterated diagonalization of the Hamiltonian in the space spanned by the present trial state $\mathfrak{P}_0 \mathbb{1}$ and its derivatives with respect to the variational parameters $\mathfrak{P}_i \mathbb{1} = \frac{\partial}{\partial \gamma_i} \mathfrak{P}_0 \mathbb{1}$. The trial-state representation for the next iteration can be represented as the Taylor expansion

$$\mathfrak{P} \mathbb{1} = \sum_{i=0}^{n_c} c_i \mathfrak{P}_i \mathbb{1}; \quad (C2)$$

where c_i is the proposed change in the parameters. The values c_i may be obtained as the solution of the generalized eigenvalue problem in this non-orthogonal and incomplete basis

$$H \mathfrak{P} \mathbb{1} = E S c; \quad (C3)$$

where S is the overlap matrix $S_{ij} = \langle \mathfrak{P}_i | \mathfrak{P}_j \rangle$. Even better results were obtained using a slightly different basis which was additionally chosen to be semi-orthogonalized with respect to $\mathfrak{P}_0 \mathbb{1}$, such that $\langle \mathfrak{P}_0 | \mathfrak{P}_i \rangle = 0; i = 1; \dots; n_c$. The stabilisation of this procedure is discussed in Ref. 67.

2. Optimization of Overlaps

Where the exact ground state is known from exact diagonalization, we may revert to a simpler method of singling out

the optimal trial wavefunction of the form (25), namely optimizing the overlap with the exact wavefunction. Here, the main difficulty lies in the evaluation of the overlap between the trial states and the exact ground state: the trial wavefunctions are known in real-space, results from exact diagonalization are given in the second quantized notations of occupation in momentum space

$$\mathfrak{P}_{\text{exact}} \mathbb{1} = \sum_{\alpha=1}^{D(L_z=0)} a_{\alpha} c_{m_1(\alpha)}^{\dagger} \dots c_{m_{N_1}(\alpha)}^{\dagger} \mathfrak{P}_0 \mathbb{1}; \quad (C4)$$

with α denoting a many-body basis state in the Hilbert subspace at $L_z = 0$ of dimension $D(L_z = 0) = D(L = 0)$, and corresponding amplitudes a_{α} . Converting trial states $\mathfrak{P}_{\text{trial}}(\{z_i; w_i\}g)$ into the second quantized basis is difficult, so overlaps are calculated in real space with a Monte-Carlo evaluation of the integral over many configurations $\sigma = (\{z_i; w_i\}g)$

$$\langle \mathfrak{P}_{\text{exact}} | \mathfrak{P}_{\text{trial}} \rangle = \int d\sigma \Psi_{\text{exact}}(\sigma) \Psi_{\text{trial}}^{\gamma}(\sigma) \quad (C5)$$

based on $\Psi_{\text{exact}}(\{z_i; w_i\}g) = \langle \mathfrak{P}_0 | \mathfrak{P}_{\text{exact}} \mathbb{1} \rangle$. Each evaluation of $\Psi_{\text{exact}}(\sigma)$ requires the evaluation of $D(L_z = 0)$ Slater determinants of size N_1 , which is the most time-consuming operation. It is therefore advised to generate a sequence of Monte-Carlo samples from the exact wavefunction only *once*, and subsequently use it to calculate overlaps with various trial wavefunctions via correlated sampling.

The optimization step of finding the value for the parameters γ_{opt} which yields the highest overlap turns out to be rather simple. The Fletcher-Reeves method (a steepest descent algorithm) was found to yield satisfactory results.

APPENDIX D: ANALYSIS OF CORRELATION FUNCTIONS

In the main text of the paper, we analyzed the energies of trial states and their overlaps with the exact trial state as a measure of their performance. Alternatively, one may use a comparison of the correlation functions as a gauge for capturing the physics of the exact solution. The correlation functions provide more information about the system, which makes them a more comprehensive measure, but also more difficult to interpret than a single number as the energy. We define the pair correlation functions⁶⁶ as

$$h_{\sigma\sigma^0}(\theta) = \frac{\mathcal{N}_{\sigma\sigma^0}}{\langle \rho_{\sigma}(\boldsymbol{r}) \rho_{\sigma^0}(\boldsymbol{r}^0) \rangle} \quad (D1)$$

where $\rho_{\sigma}(\boldsymbol{r})$ is the density in layer σ at position \boldsymbol{r} , and θ is defined as the great circle angle between positions \boldsymbol{r} and \boldsymbol{r}^0 . The normalization is chosen such that $h(\boldsymbol{r} \neq \boldsymbol{r}^0) = \mathcal{N}_{\sigma\sigma^0}$, with

$$\mathcal{N}_{\sigma\sigma^0} = [(N=2) \quad \delta_{\sigma\sigma^0} = (N=2)]; \quad (D2)$$

This choice accounts for the different number of interacting particle pairs in the interlayer and intralayer correlations.

Let us first discuss some of the physics revealed by the correlation functions in the bilayer (see also Ref. 30). Some correlation functions are shown in Fig. 10 for $N = 5 + 5$ electrons.

The top panel of Fig. 10 shows both the correlation functions at $d = 0$ and $d = 0.5 \gamma_0$. Note that for d as small as $d = 0.5 \gamma_0$, the correlation hole for small r in the intralayer correlation function $h_{\# \#}$ is noticeably enlarged with respect to the 111-state, the exact ground state at $d = 0$. The correlation hole in the interlayer correlation function $h_{n \#}$ is reduced accordingly, with $h_{n \#}(0) > 0$. We find that the observed change in the correlation functions can be understood by exclusively considering the admixture of CF to the 111-state: the mixed fluid wavefunctions (25) perfectly reproduce these correlations.

With growing d , the anti-correlations described by the correlation hole in $h_{n \#}$ continue to decrease and the correlation hole in $h_{\# \#}$ expands to its full size. For choices of g_n that correspond to sufficiently large numerical values such that the correlation hole in $h_{\# \#}$ has reached its full size, the shape of the intralayer correlation function is relatively insensitive to the precise values of these parameters. This means that intralayer correlations are coded into the Jastrow factors regardless of the specific (projected) CF orbital. In contrast, the interlayer correlation function $h_{n \#}$ has a strong dependence on the shape of g_n .

In section III A of the main text, we highlighted that paired states without an admixture of CB correlations reproduce exact ground states down to $d = \gamma_0$. As an example for a correlation function $h_{n \#}$ in this regime, the bottom panel of Fig. 10, showing $d = 1.25 \gamma_0$, features a strong anti-correlation of electrons in both layers. This correlation hole can thus be explained entirely in terms of CF-pairing, which seems counterintuitive as one would expect pairing to enhance correla-

tions between the layers. With regard to the shape of the pair wavefunctions (17) where $g(\zeta; w) \propto (\zeta - w)$ for p -wave pairing, we can more clearly understand this feature. By virtue of this property, $p_x + ip_y$ pairing introduces interlayer *anti*-correlations on short length scales. As the pair wavefunction is forced to have a maximum and to decay for $r \rightarrow \infty$, g is guaranteed to describe a bound state of pairs with some finite typical distance between the bound particles. Correspondingly, the correlation hole in $h_{n \#}$ is accompanied with an enhanced correlation around $r = 2 \gamma_0$.

In the regime of intermediate layer separation shown in the bottom panel of Fig. 10, the overlap with the exact ground state is not quite perfect [the state shown was optimized on the overlap, attaining a value of 0.987 (3) for $d = 1.25 \gamma_0$]. Optimization over either the overlap or the energy results in highly accurate correlation functions at short distances, while the large r behavior is weighted lower and may not be fully reproduced. However, as shown in Fig. 10, the correlations of the paired CF-CB states are extremely close to the exact correlation functions. For these variational state, some of the accuracy at short distances can be traded for a better reproduction of the large r behavior.

As a prominent reference case, we might cite the correlation function of the Laughlin state. Though the Laughlin state is a very accurate description of the ground state at filling factor $\nu = 1/3$, its correlation function still deviates noticeably from the correlation of the exact ground state at large r , as shown in Fig. 11.

-
- ¹ S. Das Sarma and A. Pinczuk, eds., *Perspectives in Quantum Hall effects* (Wiley, New York, 1997).
 - ² O. Heinonen, ed., *Composite Fermions* (World Scientific, 1998), for a review of CF's.
 - ³ N. E. Bonesteel, I. A. McDonald, and C. Nayak, Phys. Rev. Lett. **77**, 3009 (1996).
 - ⁴ J. P. Eisenstein and A. H. MacDonald, Nature **432**, 691 (2004).
 - ⁵ Y. N. Joglekar and A. H. MacDonald, Phys. Rev. B **64**, 155315 (2001).
 - ⁶ J. Schliemann, S. M. Girvin, and A. H. MacDonald, Phys. Rev. Lett. **86**, 1849 (2001).
 - ⁷ J. Schliemann, Phys. Rev. B **67**, 035328 (2003).
 - ⁸ A. Stern and B. I. Halperin, Phys. Rev. Lett. **88**, 106801 (2002).
 - ⁹ K. Park, Phys. Rev. B **69**, 045319 (2004).
 - ¹⁰ K. Nomura and D. Yoshioka, Phys. Rev. B **66**, 153310 (2002).
 - ¹¹ Y. B. Kim, C. Nayak, E. Demler, N. Read, and S. DasSarma, Phys. Rev. B **63**, 205315 (2001).
 - ¹² T. Morinari, Phys. Rev. B **59**, 7320 (1999).
 - ¹³ G. Möller, S. H. Simon, and E. H. Rezayi, Phys. Rev. Lett. **1101**, 176803 (2008).
 - ¹⁴ J. Ye and L. Jiang, Phys. Rev. Lett. **98**, 236802 (2007).
 - ¹⁵ R. L. Doretto, A. O. Caldeira, and C. M. Smith, Phys. Rev. Lett. **97**, 186401 (2006).
 - ¹⁶ M. V. Milovanović and Z. Papić (2007), arXiv:0710.0478.
 - ¹⁷ S. Q. Murphy, J. P. Eisenstein, G. S. Boebinger, L. N. Pfeiffer, and K. W. West, Phys. Rev. Lett. **72**, 728 (1994).
 - ¹⁸ I. B. Spielman, J. P. Eisenstein, L. N. Pfeiffer, and K. W. West, Phys. Rev. Lett. **84**, 5808 (2000).
 - ¹⁹ I. B. Spielman, J. P. Eisenstein, L. N. Pfeiffer, and K. W. West, Phys. Rev. Lett. **87**, 036803 (2001).
 - ²⁰ M. Kellogg, I. B. Spielman, J. P. Eisenstein, L. N. Pfeiffer, and K. W. West, Phys. Rev. Lett. **88**, 126804 (2002).
 - ²¹ M. Kellogg, J. P. Eisenstein, L. N. Pfeiffer, and K. W. West, Phys. Rev. Lett. **90**, 246801 (2003).
 - ²² I. B. Spielman, M. Kellogg, J. P. Eisenstein, L. N. Pfeiffer, and K. W. West, Phys. Rev. B **70**, 081303(R) (2004).
 - ²³ E. Tutuc, M. Shayegan, and D. A. Huse, Phys. Rev. Lett. **93**, 036802 (2004).
 - ²⁴ R. D. Wiersma, J. G. S. Lok, S. Kraus, W. Dietsche, K. von Klitzing, D. Schuh, M. Bichler, H.-P. Tranitz, and W. Wegscheider, Phys. Rev. Lett. **93**, 266805 (2004).
 - ²⁵ N. Kumada, K. Muraki, K. Hashimoto, and Y. Hirayama, Phys. Rev. Lett. **94**, 096802 (2005).
 - ²⁶ A. R. Champagne, J. P. Eisenstein, L. N. Pfeiffer, and K. W. West, Phys. Rev. Lett. **100**, 096801 (2008).
 - ²⁷ A. R. Champagne, A. D. K. Finck, J. P. Eisenstein, L. N. Pfeiffer, and K. W. West, Phys. Rev. B **78**, 205310 (2008).
 - ²⁸ Y. N. Joglekar, A. V. Balatsky, and A. H. MacDonald, Phys. Rev. Lett. **92**, 086803 (2004).
 - ²⁹ K. Moon, H. Mori, K. Yang, S. M. Girvin, A. H. MacDonald, L. Zheng, D. Yoshioka, and S.-C. Zhang, Phys. Rev. B **51**, 5138 (1995).
 - ³⁰ N. Shibata and D. Yoshioka, J. Phys. Soc. Jpn. **75**, 043712 (2006).
 - ³¹ N. E. Bonesteel, Phys. Rev. B **48**, 11484 (1993).
 - ³² G. Moore and N. Read, Nucl. Phys. **B360**, 362 (1991).
 - ³³ M. Greiter, X. G. Wen, and F. Wilczek, Nucl. Phys. B **374**, 567

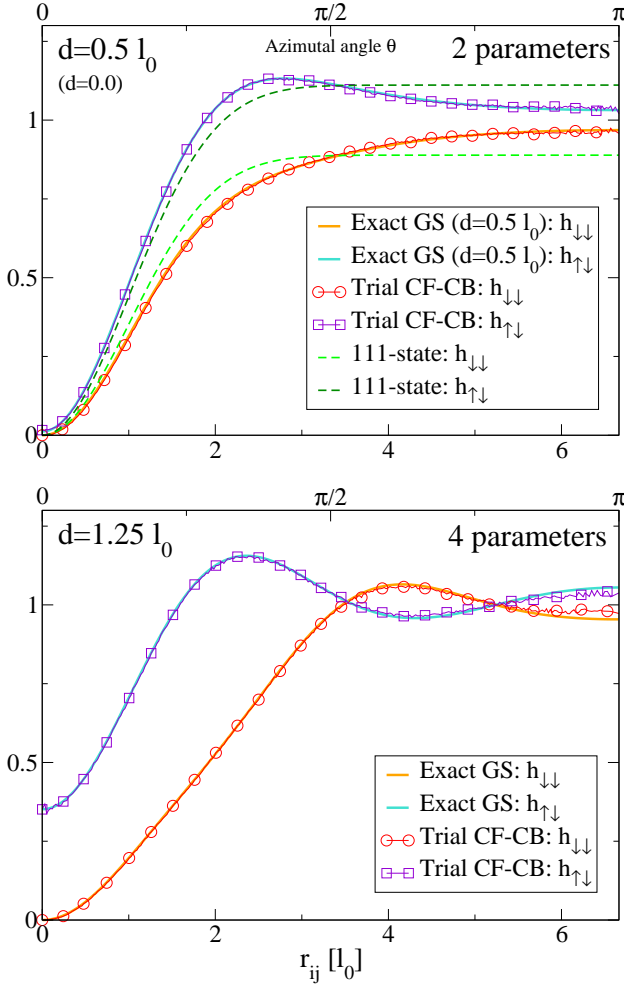


FIG. 10: Correlation functions $h_{\sigma\sigma'}(r)$ of the respective “best” trial states at layer separations $d = 0.5 \gamma_0$ (top) and $d = 1.25 \gamma_0$ (bottom) for a system with $5 + 5$ electrons. The agreement between the trial wave-functions (thin lines with symbols) and the exact results (bold lines) is significant for any value of d . Even at small finite d , the correlations $h_{\sigma\sigma'}(r)$ differ noticeably from those of the 111-state (top). The number of variational parameters employed is indicated in each case. The small noise in some of the curves for the trial states is Monte-Carlo error.

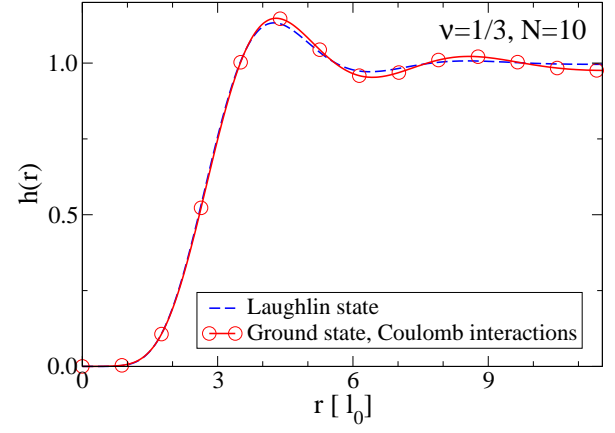


FIG. 11: Two-point correlation function $h(r)$ of the Laughlin state as it compares to that of the exact ground state for Coulomb interactions on the sphere. The good trial ground energy of the Laughlin state arises from the precise reproduction of the exact correlations at short layer separations. However, oscillations at larger layer separation have a stronger amplitude in the ground state.

(1992).
³⁴ S. H. Simon, E. H. Rezayi, and M. V. Milovanovic, Phys. Rev. Lett. **91**, 046803 (2003).
³⁵ J. K. Jain, Phys. Rev. B. **41**, 7653 (1990).
³⁶ B. I. Halperin, P. A. Lee, and N. Read, Phys. Rev. B **47**, 7312 (1993).
³⁷ R. L. Willett, R. R. Ruel, K. W. West, and L. N. Pfeiffer, Phys. Rev. Lett. **71**, 3846 (1993).
³⁸ N. Read, Semi Cond. Sci. Tech. **9**, 1859 (1994).
³⁹ K. L. Graham, S. S. Mandal, and J. K. Jain, Phys. Rev. B. **67**, 235302 (2003).
⁴⁰ G. Murthy and R. Shankar, Rev. Mod. Phys. **75**, 110 (2003).
⁴¹ N. Read, Phys. Rev. B. **58**, 16262 (1998).
⁴² A. Stern, B. I. Halperin, F. von Oppen, and S. H. Simon, Phys. Rev. B. **59**, 12547 (1999).

⁴³ J. K. Jain and R. K. Kamilla, Phys. Rev. B **55**, R4895 (1997).
⁴⁴ In Ref. 13, we had used an abbreviated notation with $\tilde{\phi}_{\mathbf{k}}$ including Jastrow factors J_i . Here, we differently chose to write the Jastrow factors explicitly to highlight the different flux attachments leading to CFs and CBs.
⁴⁵ T. Morinari, Phys. Rev. Lett. **81**, 3741 (1998).
⁴⁶ P. G. de Gennes, *Superconductivity of Metals and Alloys* (Benjamin, New York, 1966).
⁴⁷ K. Yang, K. Moon, L. Belkhir, H. Mori, S. M. Girvin, A. H. MacDonald, L. Zheng, and D. Yoshioka, Phys. Rev. B **54**, 11644 (1996).
⁴⁸ B. I. Halperin, Helv. Phys. Acta **56**, 75 (1983).
⁴⁹ T.-L. Ho, Phys. Rev. Lett. **75**, 1186 (1995).
⁵⁰ F. D. M. Haldane, Phys. Rev. Lett. **51**, 605 (1983).
⁵¹ N. Regnault, *The fractional quantum Hall effect numerical database*, <http://www.phys.ens.fr/~regnault/qhe/>.
⁵² D. Yoshioka, *The Quantum Hall Effect*, Series in Solid-State Sciences, Vol. 133 (Springer, 1998).
⁵³ E. Rezayi and N. Read, Phys. Rev. Lett. **72**, 900 (1994).
⁵⁴ M. V. Milovanovic, Phys. Rev. B **75**, 035314 (2007).
⁵⁵ G. Möller and S. H. Simon, Phys. Rev. B **77**, 075319 (2008).
⁵⁶ To illustrate the meaning of the variational parameters g_n more clearly, we provide a discussion of the point in the online supplementary material to this paper, Ref. 57.
⁵⁷ G. Möller, S. H. Simon, and E. H. Rezayi, EPAPS Document No. E-PRBMDO-79-086908. For more information on EPAPS, see <http://www.aip.org/pubservs/epaps.html>.
⁵⁸ N. Read and D. Green, Phys. Rev. B **61**, 10267 (2000).
⁵⁹ F. D. M. Haldane and E. H. Rezayi, Phys. Rev. B **31**, 2529 (1985).
⁶⁰ Y. N. Joglekar and A. H. MacDonald, Phys. Rev. B **65**, 235319 (2002).
⁶¹ I. B. Spielman, L. A. Tracy, J. P. Eisenstein, L. N. Pfeiffer, and K. W. West, Phys. Rev. Lett. **94**, 076803 (2005).
⁶² G. Fano, F. Ortolani, and E. Colombo, Phys. Rev. B **34**, 2670 (1986).
⁶³ I. Tamm, Z. Physik **71**, 141 (1931).
⁶⁴ T. T. Wu and C. N. Yang, Nucl. Phys. **B107**, 365 (1976).
⁶⁵ T. T. Wu and C. N. Yang, Phys. Rev. D **16**, 1018 (1977).

⁶⁶ We choose to represent the pair correlation function using the symbol $h(r)$ for the entirety of this paper, since $g(r)$ is used as a symbol for the pair wavefunction.

⁶⁷ C. J. Umrigar, J. Toulouse, C. Filippi, S. Sorella, and R. G. Hennig, Phys. Rev. Lett. **98**, 110201 (2007).